Fault Detection and Tolerance of Electrical Machines in Automotive Applications

By Gary Buckley

Submitted to The University of Nottingham for the degree of Doctor of Philosophy

2017

Contents

i. Table of Figures iv

ii. Table of Acronyms viii

iii. Table of Symbols ix

iv. Abstract x

1 Introduction 1

1.1 Overview 1

1.2 Industrial links 7

1.3 Objectives 9

1.4 Statement of originality 13

1.5 Thesis Layout 14

2 Review of Current Literature 16

2.1 ISO26262 Road Vehicles – Functional Safety [5] 16

2.2 Rotor Magnet Temperature Monitoring 19

2.3 Sensorless Rotor Position Measurement 35

2.4 Conclusion 48

3 Simulation of a Sensorless Control System Based on Fundamental PWM Transient Excitations 51

3.1 SVPWM Generation Block 52

3.2 Derivative Current Sensing 55

3.3 Position Estimation 56

3.4 Simulation Results 56

3.5 Conclusions 58

4 Development of an innovative Magnet Condition Monitoring Scheme 59

4.1 Derivation of Magnet Condition Monitoring Model 59

4.2 Simulation of Magnet Condition Monitoring Scheme 62

4.3 Conclusions 72

5 Development of Stator Impedance Monitoring Scheme 74

5.1 Fault Definition 74

5.2 Analysis of Faulted Machine 76

5.3 Conclusions 82

6 Experimental Results 83

6.1 Experimental Rigs 83

6.2 Implementation of Magnet Condition Monitoring 86

6.3 Initial Position Detection Scheme 93

7 Conclusions 97

8 Further Work 100

9 References 103

Appendix A: Review of ISO26262 115

i. Table of Figures

Figure 1: Basic hybrid drive topologies (a) Series hybrid, (b) Parallel hybrid [4] 3

Figure 2: Cummins radial flux motor generator [10] 8

Figure 3: Sectioned rotor highlighting skewed buried magnets [10] 8

Figure 4: Key traction machine parameters [10] 9

Figure 5: ISO26262 - Content diagram. [4] 18

Figure 6: Example B-H Curve from Arnold Magnetics for an NdFeB magnet. [16] 20

Figure 7: Test pulse switching states 27

Figure 8: Proposed thermal model with two thermal nodes, i.e., permanent magnets p, stator winding s; the stator core temperature is an input quantity to the model [23] 30

Figure 9: Buried PM machine showing d and q axis. Effective air gap extension visible along d-axis 37

Figure 10: Current waveform during PWM transients 40

Figure 11: Position signal extraction from a delta wound machine 41

Figure 12: Diagram of a position and speed demodulation system 44

Figure 13: Mechanical observer with position error feedback tuning 45

Figure 14: MRAS system block diagram 47

Figure 15: Block diagram of the simulated control system 52

Figure 16: Left: The space vector plane with all vectors and sectors highlighted. Right: A voltage demand in sector 1 and the vector sequence applied to achieve it 53

Figure 17: A symmetrical PWM waveform constructed from active and zero vectors 54

Figure 18: Simulation results showing the actual and estimated position and speed of a machine subjected to a stepped speed demand followed by a load disturbance 57

Figure 19: Phasor diagram of a PM synchronous machine..... 60

Figure 20: Constant temperature test. Top: Rotor speed, Middle: Measured Iq and Back-EMF Estimate, Bottom: Actual magnet temperature and observer magnet temperature 67

Figure 21: Heat run test. Top: Constant Speed and Load. Bottom: Actual winding temperature, actual magnet temperature and observer magnet temperature. 68

Figure 22: Stator resistance sensitivity test. Magnet temperature error Vs % error in Rs..... 69

Figure 23: Voltage error sensitivity test. 70

Figure 24: Current sensing error test. 71

Figure 25: Delta winding with n parallel coils. 75

Figure 26: Per phase equivalent circuit of a parallel wound machine. 77

Figure 27: Terminal voltages for healthy and faulted machines under no load conditions 80

Figure 28: Terminal voltages for healthy and faulted machines under loaded conditions 80

Figure 29: Magnetic field density plot of the faulted machine (open coil highlighted) under load conditions. 81

Figure 30: Developed torque (per unit) for a healthy and faulted machine under load conditions over one electrical cycle. 82

Figure 31: University of Nottingham test facility 84

Figure 32: Encoder mounted on rear of the test machine 85

Figure 33: Test bed at Cummins Generator Technologies, Stamford 86

Figure 34: Iq vs. Torque. Id=0 control, constant rated speed. 88

Figure 35: Estimated Speed Constant vs. Rotor Temperature. Trended Series - 30kW, Id = 0, rated speed. Square - 15kW, Id = 0, rated speed. 89

Figure 36: Error in Speed Constant vs. Load Level. Id = 0 control, constant rated speed. 90

Figure 37: Settling time for HF-injection at start-up 93

Figure 38: Effect of d-axis voltage pulses 94

Figure 39: Experimental measurement of current response along positive and negative d-axis 96

Figure 40: Safety Life Cycle [4] 116

Figure 41: Severity ratings [4] 119

Figure 42: Probability ratings [4] 119

Figure 43: Controllability ratings [4] 120

Figure 44: ASIL determination [4] 120

Figure 45: : Product design v-cycle 122

Figure 46: Reference phase model for the product development at the hardware level 125

ii. Table of Acronyms

ADC	Analogue to digital converter
ASIL	Automotive Safety Integrity Level
DSP	Digital signal processor
EMC	Electromagnetic compatibility
EMF	Electro-Motive force
EV	Electric Vehicle
FEA	Finite Element Analysis
FMEA	Failure Mode Effect Analysis
FPGA	Field programmable gate array
HF	High Frequency
ICE	Internal Combustion Engine
IGBT	Insulated Gate Bipolar Tranistor
IPM	Interior Permanent Magnet
IR	Infra-Red
ISO	International Organsation for Standardization
KSI	Killed or seriously injured
LUT	Look-up Table
MRAS	Model Reference Adaptive System
MTPA	Maximum Torque Per Amp
PEMC	Power Electronics Machines and Controls
PI	Proportional - Integral
PID	Proportional- Integral - Derivative
PMSM	Permanent Magnet Sychronous Machine
PWM	Pulse Width Modulation
SVPWM	Space Vector Pulse Width Modulation

iii. Table of Symbols

B_{r0}	Residual flux density at ambient temperature
d_i/d_t	Derivative of current
I_a	Current in phase a
$i_{\alpha\beta}$	Current vector in the static alpha beta reference frame
I_b	Current in phase b
I_c	Current in phase c
I_d	d-axis current
I_q	q-axis current
K_{cu}	Coefficient of resistivity for copper
K_d	Derivative gain
K_{emf}	Back-emf constant
K_i	Integral gain
K_p	Proportional gain
K_t	Torque constant
$L_{\alpha\beta}$	Machine inductane in the static alpha beta reference frame
L_{coil}	Inductance of a coil
L_d	d-axis inductance
L_d'	d-axis incremental inductance
L_q	q-axis inductance
L_q'	q-axis incremental inductance
μ_0	Permeability of free space
ϕ_m	Magnet flux
ϕ_r	Rotor flux
$\phi^s_{\alpha\beta}$	Stator flux vector in the static alpha beta reference frame
R_{coil}	Resistance of a coil
T_0	Ambient temperature
θ_e	Electrical rotor angle
v_a	Voltage of phase a
v_{abc}	Three phase voltage signal
$v_{\alpha\beta}$	Two phase equivalent voltage signal
v_b	Voltage of phase b
v_c	Voltage of phase c
v_d	d-axis voltage
V_{dc}	DC-Link voltage
v_q	q-axis voltage
v_s	Stator voltage
$V^s_{dq\_hf}$	High frequency stator voltage in the rotating dq reference frame
ω_c	Carrier signal frequency
ω_i	Signal injection frequency
ω_r	Rotor speed
Z^s_{dq}	High frequency impedance in the rotating reference frame

iv. Abstract

This project explores the drive for further electrification in the automotive industry and the challenges that this brings. Specifically this thesis focuses on the demands of safety and reliability; highlighting the subtle difference between the two concepts, explaining how legislation is forcing designers to consider the ways in which a system could fail and requiring them to create methods to detect and safely handle these failures, many of which can never be completely eliminated by design.

With this motive in mind, the research within this thesis is focused on fault detection and condition monitoring. A novel method of rotor magnet condition monitoring is developed, an investigation into the effects of stator impedance variation is carried out to identify opportunities to develop diagnostic algorithms and sensorless control is considered as a back-up control method should a traditional position sensor fail.

This thesis shows how current research and new techniques could be applied in the modern automotive industry; highlighting the demand for ever safer electronic systems as the world strives for greater levels of autonomy on the roads.

1 Introduction

1.1 Overview

The automotive industry is seeing an increasing reliance on electrical drives and electronic technologies as it aims to increase efficiency, safety and comfort [1] [2] [3]. Technologies are being developed to provide traction, safety and comfort such as hybrid drives, electronic power steering, climate control, driver navigation, driver assists and electric turbochargers all need energy supply or management systems.

1.1.1 Levels of electrification

There are varying levels of electrification currently implemented on vehicles within automotive market. This ranges from a traditional internal combustion engine (ICE) driven vehicle to all electric solutions, some of these topologies are described below.

1) **Traditional ICE driven vehicle**

   In a traditional passenger car the engine drives the wheels through a clutch and gearbox. There is usually a small alternator and a 12V battery to power the auxiliary electronic items on the vehicle, for example lights or radio.

2) **Hybrid electric vehicle**

   A hybrid electric vehicle is one which contains both an ICE and an electric traction machine. The current selection of hybrid vehicles in the market can be derived from one of two basic topologies, series or parallel hybrids.

a. Series hybrid vehicles

A series hybrid vehicle uses the ICE as a generator to charge a large battery and a traction machine to drive the wheels. The electric machine can also recharge the battery under braking. A series hybrid vehicle topology can be seen in Figure 1.

b. Parallel hybrid (Figure 1)

In a parallel hybrid system the ICE is used to provide traction as well as charge the batteries from a traction machine. The electric machine is then used to provide a boost to the ICE torque under acceleration and can be used to regenerate energy under braking. A parallel hybrid topology also offers the opportunity to use the traction motor to start the ICE.

3) All-electric vehicles

As the name implies, an all-electric vehicle does not use an ICE, all traction being provided by an electric machine driven from batteries or fuel cell technology.

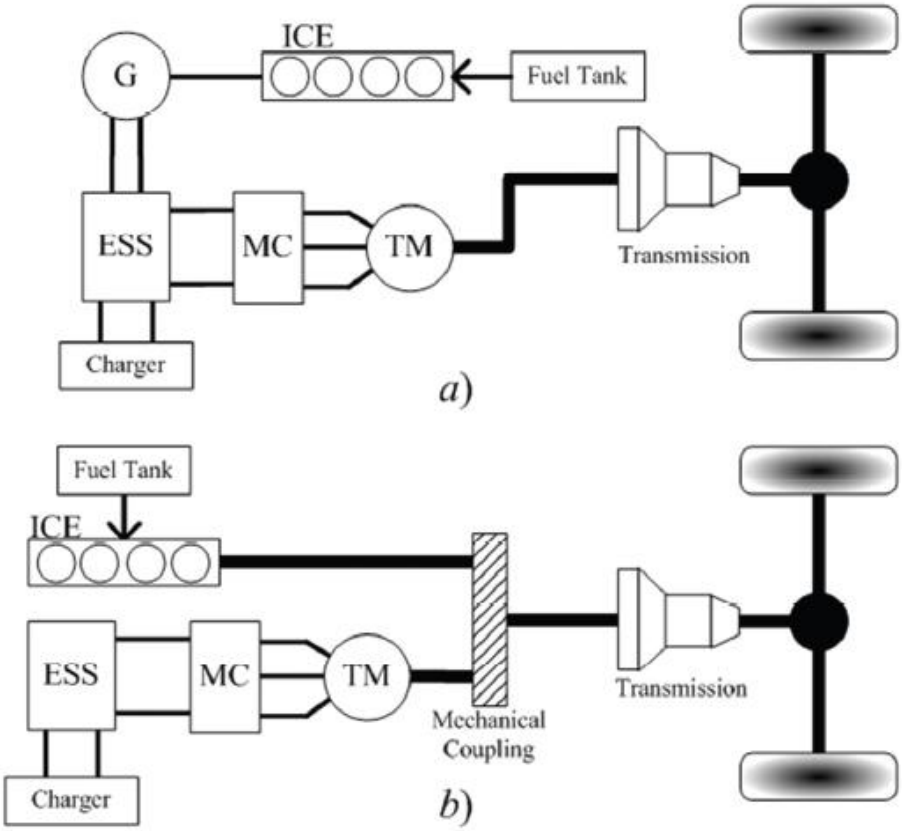

Figure 1: Basic hybrid drive topologies (a) Series hybrid, (b) Parallel hybrid [4]

These various applications put different demands on the technical solution, for example a traction motor to propel an all-electric or hybrid vehicle will have very large power and torque requirements. If replacing an internal combustion engine completely, this often forces the use of higher voltages than traditionally found in a vehicle. Other applications such as a power steering drive has a much lower power demand; but the torque ripple and physical size constraints to integrate with the rest of the steering system and package within the dashboard of a vehicle offers other challenges. These various applications all require different solutions from traction

machines needing to provide very high levels of torque to an advanced electrical machine housed in a turbo which must handle extremely high speeds and temperatures.

1.1.2 Increased demands

Traditionally, supplying the smaller electrical systems found in a vehicle is the job of the alternator; a small and relatively cheap electrical machine which is belt driven from the prime mover and charges a 12 or 24V battery. However each of these technologies, be it a small driver navigation system or a large hybrid drive, require energy to perform their functions. This in turn raises the overall demand on power within the vehicle and this trend only looks set to continue and so generation and energy storage methods must also increase to match. Options are being developed and implemented within the automotive industry to provide more charge to the battery by recovering wasted energy from the internal combustion engine and vehicle dynamics. Examples of this kind of generation are; kinetic energy recovery as seen on hybrid vehicles and in Formula 1 racing where an electrical machine which can be used for traction is also used to brake the vehicle and so generating power; this technology is perhaps the most familiar within commercial and domestic vehicles where a large machine in the driveline is used to harvest energy as the vehicle is braking. Another recovery method is to have high speed machines which operate on the turbo shaft; these machines can recover energy from the exhaust stream and can also be used to boost the engine pressure and reduce turbo lag to improve engine pressure and efficiency, these systems demand high levels of manufacturing precision and operate at extremely high speeds and temperatures, for this

reason they are mainly found in motorsport environments and far less in road vehicles.

The future trend must be an increased utilisation of these and similar electrical drive systems within the automotive industry. The benefits of this are twofold; allowing the ever increasing demand for technology within vehicles and the inevitable power supply demands that this brings, secondly these systems can be used to improve the overall vehicle efficiency and so reducing the consumption of fossil fuels and the emission of harmful gasses.

1.1.3 Drive for fault tolerance and detection

Many of these new technologies are applied in safety critical areas of the vehicle; attached to the drive train, steering or braking systems for example. This means that the safety and reliability requirements on such systems are very demanding. This can be seen by analysing new legislation introduced to standardise the risk assessment and design processes of safety critical automotive systems, for example ISO 26262 Road Vehicles – Functional Safety [5]. This standard was introduced by the International Organisation for Standardization to offer a standard approach to the management of functional safety within automotive electrical and electronic systems – simply put; the standard ensures a consistent and auditable approach to designing safe automotive electrical systems. The scope and requirements have far reaching impacts on both the design of automotive electronic products and the responsible engineering organisation. A common solution to the safety question is to add in redundancy to maintain the availability of a system even if a fault is present; for an electric machine this is often in the form of multiple phases controlled from multi-leg or

completely separate power electronic converters [6] [7] [8]. The obvious problem with redundancy is the additional cost and technology which lies redundant for the vast majority of the product's operation; in an automotive environment where weight and cost are key market drivers a vehicle manufacturer does not wish to carry redundant components. This is where other techniques such as the fault detection and back-up control discussed in this thesis can help; allowing the system to fall into a safe state or operate on reduced output until the driver can bring the vehicle to a safe stop without the need for doubling up expensive, heavy components.

A common trend within industry is to take advantage of the favourable power densities offered by permanent magnet synchronous machines (PMSM) in order to meet the high demands on both package size and weight present in modern automotive system design [9]. Maintaining optimum closed loop control of a system built around a PMSM requires knowledge of the condition of the rotor of the machine. The first and most obvious parameter of interest is the physical rotor angle; without which the angle of a voltage vector and so stator field which must be applied to result in the requested rotor torque cannot be accurately determined.

An incorrect rotor angle can lead to various conditions including rotor locking and reversed or erratic motion, in safety critical automotive systems this is clearly an unacceptable condition. An example could be a power steering motor which applies a reversed force, this would effectively 'fight' the drivers input making it difficult or impossible to steer the vehicle. In a traditional system the rotor angle is provided by use of an encoder or a resolver fitted to the machine, these devices can be extremely accurate and when used in a well-tuned vector control system can offer very good

performance; however an issue arises when the device or its interconnection within the system fails.

1.2 Industrial links

This project has close links to an industrial partner. Much of the work contained within this thesis has been performed in parallel with the partner's development of a commercial vehicle hybrid drive. The majority of the simulation and experimental work described have been carried out on the associated machine and its topology has been critical in determining some of the faults considered and also in shaping some of the detection and monitoring techniques proposed.

1.2.1 The traction machine

The machine shown in Figure 2 is the 16 pole, 24 slot interior permanent magnet machine developed by Cummins Generator Technologies [10] around which the majority of work in this thesis is based. The winding topology employed is a 3 phase delta winding with 8 independent parallel concentrated coils per phase. The 8 coils are connected to a series of end rings within the machine and three terminal connections are then offered to the terminal block along with the signal from a thermocouple buried within the windings and the signals from an integrated rotor position resolver.

Figure 2: Cummins radial flux motor generator [10]

The laminated rotor shown in Figure 3 is made of 5 stacks containing NdFeB magnets, each offset to form a skew along the rotor axis. These are held in place by aluminium end rings and mounted on a single bearing within the two part stator housing, which is designed to contain a water cooling jacket around the stator windings.

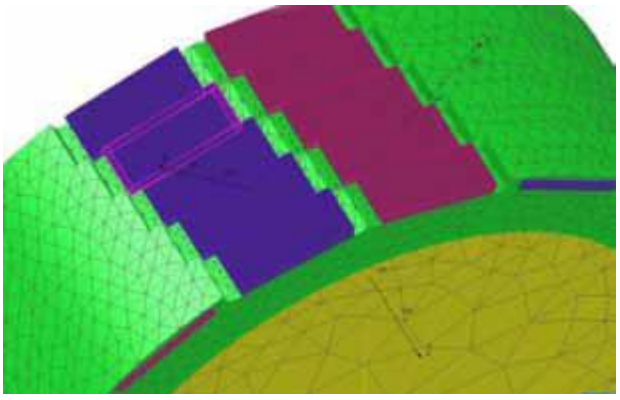

Figure 3: Sectioned rotor highlighting skewed buried magnets [10]

The machine is designed to sit in the main drive train between a diesel engine and gearbox. It is also designed with the ability to act as a start stop machine, so must deliver very high torque for short periods of time to start

a potentially frozen (-40°C) commercial vehicle engine. The industrial partner addressed this requirement by increasing the back iron to avoid saturation during very high loadings (greater than 3x operating currents). The main parameters of the machine can be observed in Figure 4.

Peak Torque (60sec)	660 Nm
Peak Power (60sec)	90 kW @ 1300rpm
Continuous Power	35-40 kW @ 1300rpm
Efficiency	> 95 %
Length	200 mm
Diameter (Interface)	SAE 2
Mass	108 kg
Cooling	Water/Glycol, 12 l/min
M/G Inertia	0.41 kg-m2
Cogging Torque (Pk-Pk)	15.2 Nm
Max. Current @ 660Nm	418 A
Short Circuit Current	275 A
Position Sensor	Resolver
Temperature Sensor	2 x RTD PT1000
Safety	High voltage interlock in terminal box cover

Figure 4: Key traction machine parameters [10]

1.3 Objectives

This thesis will initially look further into the safety demands on electric drive systems and the organisations designing them for the automotive industry

and will look at examples of where ISO26262 applies, specifically what it requires of a designer and how fault detection and condition monitoring methods can be used in order to meet these requirements. The thesis will then offer solutions to some issues often faced by designers of electric drives within the automotive industry.

The first instance will be to review sensorless control methods which could be utilised should a failure occur in the rotor position sensing technology; these methods allow the rotor position to be derived by using the control circuitry to interrogate the permanent magnet machine with high frequency signals or by monitoring parameters as part of a model based scheme. Some of these techniques will then be implemented in detailed simulations and an initial position detection scheme will be implemented experimentally. The techniques could then be used as a comparison to detect a fault within the standard angle measurement system and also to provide a substitute signal; allowing a safety critical system to operate in a back-up mode which would enable a user to safely bring the vehicle to a stop or even to drive it home or to a garage for service.

The thesis will then focus on the electric machine itself. Two particular fault groups will be targeted; stator impedance variations and rotor magnet faults. The project will attempt to develop techniques to monitor the condition of these machine parameters enabling the early detection and diagnosis of such faults. Such detection could enable the system to be brought to a safe state before a catastrophic failure lead to a loss of control.

A challenge of using rare earth permanent magnets is their varying performance and potential permanent demagnetisation at high

temperatures. This means that the temperature of the rotor is an important parameter to be aware of if reliable, safe performance is to be maintained. This thesis will review current methodologies for overcoming this challenge, looking into estimation and measurement techniques to determine the temperature of the rotor magnets.

It will then develop a novel technique; firstly through simulation and then experimentally to monitor rotor magnet condition. This technique in combination with a commissioning and tuning process could be used to monitor magnet temperature and so assist a suitable derating strategy to protect them as well as offer a check against more permanent damage such as cracks.

The second machine fault is a stator impedance variation; in the particular system on which this project is primarily focussed the machine is a delta wound permanent magnet machine with 8 parallel coils per phase. Due to the nature of its construction a possible failure mode in extreme conditions is for one of the connections to break causing a single open coil. This failure mode will be investigated through simulation to assess its impact and how detectable the effects are.

In summary the key objectives are this work are to;

1. Investigate the impacts of safety legislation on electric drive developments and other electronic technologies within the automotive market.
2. Review current literature and offer proposals of additional monitoring and fault detection methods which could be valuable in satisfying the above legislation.

3. Demonstrate or develop these methods in simulation or experimental environments.

The following sections of this thesis will refer back to these objectives, showing where each is addressed. Throughout the thesis objectives 2 and 3 are further broken down into detailed elements which will in turn satisfy the larger objective.

The reviewing phase (objective 2) will look specifically at;

- Rotor magnet condition monitoring, considering both temperature and magnetisation fluctuations.
- Rotor position estimation techniques to serve as a monitoring tool or back-up mode for a standard position sensor or potentially to replace the sensor itself.

The derivation and implementation phase (objective 3) will then comprise of;

- Investigation of rotor position sensing techniques in simulation (chapter 3) and experimental validation of an initial position detection scheme (chapter 6.3)
- Derivation of a novel rotor magnet condition monitoring scheme (chapter 4)
- Experimental validation of the rotor magnet condition monitoring (chapter 6.1)
- Investigation of a detection scheme for a stator winding fault identified during the machine development (chapter 5)

1.4 Statement of originality

This project is attempting to derive and offer solutions to specific issues in implementing an automotive electric drive system in line with current automotive legislation and standards (Objectives 1 and 2). In the domain of functional safety it is essential to be able to detect, in real time, the onset of certain faults and to be able to mitigate any unsafe reaction they cause. This detection must be carried out robustly and without affecting the performance of the machine itself. It also must meet the stringent guidelines around electronic components within an automotive environment, perhaps most challenging being the electromagnetic compatibility standards demanded by most vehicle manufacturers [11] [12]. Finally they must be implemented on systems with relatively low microprocessor overhead; cost is a key driver within the automotive industry and so there is great pressure to implement simple, elegant and cheap solutions.

In the spirit of safety engineering, this project will focus on faults which could cause safety critical situations in a vehicle environment, so monitoring elements of a drive design which can have a direct influence its controllability. The rotor elements of a machine (position and magnet condition) are two such areas; the need to pass information from the rotating element to a static element in order to process it makes them inherently difficult to monitor. This thesis will explore the current state of the art and then through simulation and experimentation will explore possible solutions, both recognised and novel (objective 3).

Current rotor magnet monitoring techniques rely on complex thermal models with high processing demands or requiring the knowledge of detailed

boundary and initial conditions, others interrogate the machine using high frequency current or voltage injections which could dramatically affect electromagnetic compatibility and audible noise emissions due to the additional 'noise' injected. The novel solution offered in this thesis is tailored to an automotive application where pre-commissioning and tuning are common place; an algorithm is developed to derive the rotor magnet condition in real time following an initial commissioning process.

As described in Section 1.2 this project has close links with an industrial partner and has been carried out in parallel to the development of the hybrid drive machine on which much of this work is performed. During the development of the machine a particular fault was found following testing which lead to the work in chapter 5. The stator impedance fault investigated within that chapter is unique to the machine topology and so not previously investigated. The investigation carried out looks to firstly characterise this failure mode and identify the impacts and potential detection methods.

1.5 Thesis Layout

In chapter 2 this thesis will first summarise the current literature and legislation around the objectives outlined above by discussing the impacts and demands of legislation on the implementation of electronic and electrical drive technologies in the automotive industry. It will then go on to review current techniques for monitoring the temperature and condition of rotor magnets in permanent magnet synchronous machines. Finally it will review sensorless control techniques which may be suitable for use in fault monitoring or back-up control modes for automotive systems.

The thesis will then go on to investigate fault detection in electric drive systems in the following chapters. Chapter 3 will focus on the simulation of a sensorless control technique which modifies the fundamental PWM excitation in order to extract information about the rotor position. Chapter 4 explains the theoretical development of a novel rotor magnet condition monitoring technique; explaining the fundamental principles backed up with simulated results. Chapter 5 then investigates how a variation in stator impedance could be detected in real time; such a technique would allow a system to derate or to alert a driver that service is required before thermal runaway or another catastrophic failure mode could take hold. Next, the experimental conditions will be described. This work has been carried out in collaboration with commercial partners and using their hybrid drive machine, developed controllers and test facilities, details will be provided in chapter 6.

Chapter 7 will explain the experimental implementation of the magnet condition monitoring technique and explain the related tuning and commissioning process which would need to be completed on the final system. It will then describe the experimental implementation of the sensorless control techniques and describe any further work required to commercialise and implement the technique in an automotive product; highlighting any challenges which would still need to be addressed.

The thesis will then be drawn to a close with conclusions on the work presented and discussions around further work which is required in this area to enable and support the industry push towards further automation on roads around the world.

2 Review of Current Literature

Road users face risks each and every time they take to the highways across the world. There were over 190,000 reported road casualties in UK alone in the 12 months to September ’14, over 12% of which were classified as ‘Killed or seriously injured’ (KSI) casualties [13]. It should be the responsibility of the authorities managing the roads, each individual road user and also the designers and manufacturers of road vehicles to ensure that the risk to public road users is kept as low as feasibly possible.

This challenge is met in two ways; first is through legislation which will allow the effectiveness of a design with respect to public safety to be measured and monitored, an example being ISO26262 Road vehicles – Functional safety [5] which will be discussed in the initial part of this chapter. The second is by research and development of techniques which will allow unsafe faults within systems to be detected and where possible mitigated.

2.1 ISO26262 Road Vehicles – Functional Safety [5]

The aim of ISO26262 is to assist automotive organisations to avoid these risks by setting appropriate requirements and processes to prevent systemic and random hardware failures leading to hazardous situations. As described by Edwards in [14] where the author discusses the application of ISO26262 at a silicon and software level, legislation is driving a change in the way engineers must think about their designs and this also applies at a system and drive level. It is accepted that random failure can happen in any system, no matter how well designed. The standard sets out a process to assess the

effect and risk of each possible failure before setting requirements on how this risk is dealt with.

In the introduction to the standard the authors state that ISO26262 [5];

a) Provides an automotive safety lifecycle (management, development, production, operation, service, decommissioning) and supports tailoring the necessary activities during these lifecycle phases;

b) Provides an automotive-specific risk-based approach to determine integrity levels [Automotive Safety Integrity Levels (ASIL)];

c) Uses ASILs to specify applicable requirements of ISO 26262 so as to avoid unreasonable residual risk;

d) Provides requirements for validation and confirmation measures to ensure a sufficient and acceptable level of safety being achieved;

e) Provides requirements for relations with suppliers.

The remainder of this chapter will explain how the standard achieves these five points, and what it means for the design and management processes for a compliant organisation.

2.1.1 Scope

The standard itself is delivered in 10 parts as shown in Figure 5. The structure of the figure is explained in detail in appendix A; the numbering indicates the parts and chapters of the standard as a content table would. The first part of the standard acts as a glossary of terms to be used in the following parts which does not require much explanation in this thesis. Therefore, a detailed discussion of the standard will begin at part 2. Part 10

is a guideline to the implementation of the standard and so will also not be analysed in detail in this thesis.

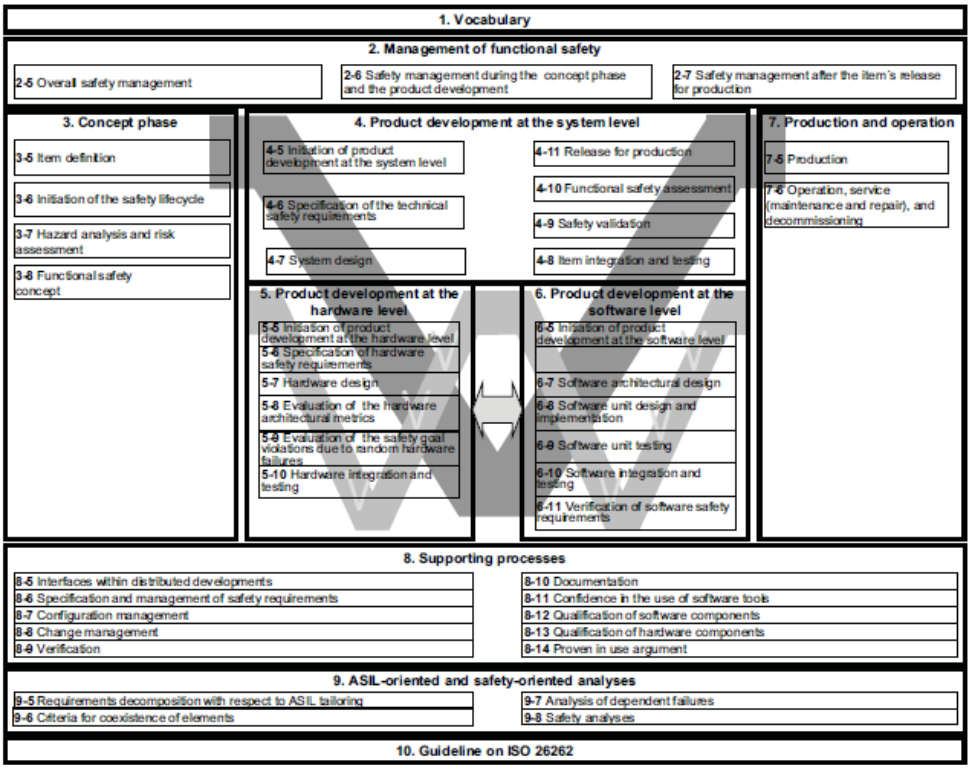

Figure 5: ISO26262 - Content diagram. [4]

The remaining sections of the standard describe in a high level of detail how functional safety affects and must be considered across every aspect of a product design and also the designers' organisation. It describes tools which should be used to give an objective and measurable indication of the safety of an electronic system, offering guidelines on how these tools are used to create requirements for sub-system design and how these should be passed through the project cycle and verified and validated before the product can be released and declared safe.

2.1.2 Conclusion

This section has provided an insight into the rigour and detailed safety analysis required when attempting to implement any new design iteration within the automotive industry. The information above and contained in the later appendix was used as justification for the techniques implemented in this work. Chapters 4 and 5 describe proposed methods of fault detection which could be offered to predict unstable behaviour and allow the system to react in a safe way to mitigate the unsafe action. Chapters 3 and 7 propose a control method utilised to provide a safe system response to a collection of failures causing a loss of rotor position measurement. These techniques can be used to reduce the number of hardware failure which can lead to ASIL D rated hazards as defined in part 3 of ISO 26262. Appendix A contains a detailed review of the standard and describes tools which can be used to assess, measure and qualify the above techniques and their contribution to the functional safety of an electric drive system.

2.2 Rotor Magnet Temperature Monitoring

The particular faults of interest for this thesis are related to permanent magnet synchronous machines; first being monitoring of the magnets themselves, secondly monitoring and back-up control for the rotor position sensing components and finally a look at the detection of stator winding impedance variation which could be caused by short or open circuit connections in multiple series or parallel wound machines. The current state of the art for the detection and monitoring of the rotor elements will be covered in this section.

The condition of magnets in a PMSM is critical to the performance of the machine. The performance of a permanent magnet is defined by its temperature dependant B-H characteristic (Figure 6). As the magnet temperature increases then the intrinsic coercivity (H) and the residual flux density will reduce. In [15] it is shown that this has a direct effect on the maximum torque which can be developed by a PMSM.

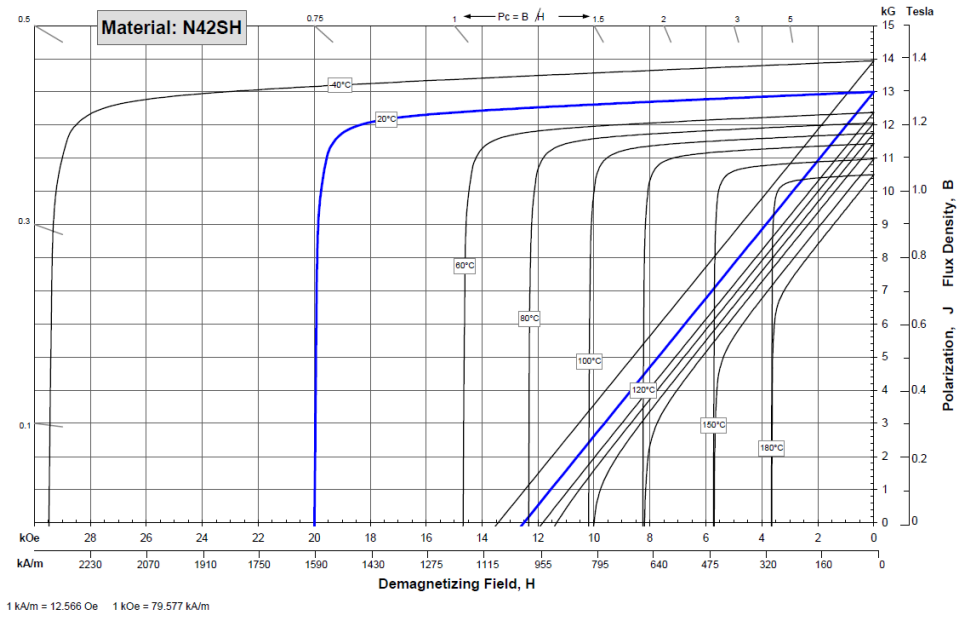

Figure 6: Example B-H Curve from Arnold Magnetics for an NdFeB magnet. [16]

In normal operation, the residual flux density and intrinsic coercivity return to normal levels when the temperature falls again. However, if the temperature increases too much (approximately 150°C for NdFeB magnets) then this can drive the operating point of the magnets into the non-linear region of the B-H curve and cause a partial or total demagnetisation.

This makes the magnet temperature a very useful parameter for the control and protection of permanent magnet machines. Unfortunately, it is a very difficult parameter to measure during operation. The methods to obtain this measurement, or an estimation of it, have been quite widely investigated in literature over recent years and methods can be separated into three categories. Firstly, methods which involve direct measurement of the temperature. Secondly, methods which involve some form of extra excitation of the stator coils in order to extract information and finally, model based methods which run in parallel with the machine control in order to monitor the magnet condition.

The following sections will describe some of the current methods in industry and research environments which can be used to obtain a rotor temperature.

2.2.1 Magnet Temperature by Direct Measurement

Direct measurement of the temperature of stator windings is fairly common in the production of rotating machines; this is done by way of thermocouples embedded within the slot along with the winding coil. This is often used as a measure of machine condition and de-ratings are calculated based on this measurement. It is however preferable, for reasons stated above, to have similar information about the temperature of the rotor. For induction machines this is to aid calculation of the rotor time constant [17], and for a permanent magnet machine it is to calculate the maximum available torque and to avoid demagnetization [15].

It would be little effort to insert thermocouples into the rotor pack in contact with the magnets during manufacture. The obstacle lies in transmitting the information from the rotating shaft out to the power electronics.

There are possible solutions to this problem, [18] and [19] suggest the use of slip rings. This option could be effective in a laboratory environment given the low demands on space and maintainability, however in operation and especially in harsh or difficult environments this is an extra component prone to wear which will reduce reliability and add cost and complexity to the machine.

In [20], [21] and [22] wireless transmission methods using different mediums are presented. All of these techniques involve having circuitry and antennae on the rotating parts of the machine. This adds a lot of complexity during the build process and will also increase the difficulty in balancing the machine. This aside, the control electronics must also be equipped to receive the wireless transmission adding costs here too. And a final consideration is any interference with surrounding systems which may be relevant in aerospace, marine or automotive applications.

In [23] a contactless method of measurement is discussed using infrared sensors. Despite sounding like a simple solution the reality is actually extremely complex and can only ever give the rotor/end ring surface temperature meaning that for the case of buried magnets/rotor bars the temperature of the material of interest must still be estimated. In order to obtain actual temperatures from the IR sensor it must be very precisely located and focused so as not to see interference from surrounding surfaces. The colour, roughness and material of the measurement surface must be

known to enable accurate calculation of the emissivity of the surface so to calibrate the probe and measurements correctly. This all increases cost and complexity requiring extra circuitry and signal processing as well as a stator housing designed to incorporate an accurately positioned sensor.

The conclusions to be drawn from this are that direct measurement with the use of contact temperature sensors offer the benefit of high accuracy, but the added complexity required in the machine and control to extract this information from the rotating parts makes this impractical for most applications. The use of infrared sensors eliminates this problem, while still giving a direct measurement. However this direct measurement is of the rotor surface, not the magnets and obtaining an accurate absolute temperature proves extremely difficult given the knowledge and condition of the measurement surface which is required.

2.2.2 Temperature Measurement by Enhanced Excitation

Various sensorless control techniques have been developed working on the principle of saliency tracking [24] [25] [26]. These techniques all rely on the extraction of information about the variation of the stator impedances with respect to the rotor angle. The pattern of the variation is known as the saliency pattern of the machine. A saliency pattern is caused by the effective uneven air gap of the machine and the change of magnetic saturation due to the location of the rotor flux vector. This rotor flux vector is set by the magnets in a permanent magnet machine, and so tracking the saturation caused by it will effectively track the magnet position forming the basic principle of these techniques.

If the residual flux density of the magnet was to reduce, as happens with increasing temperature, then the rotor flux vector would also reduce. This change could then be detected as a small change in the stator impedances using similar techniques to those developed for sensorless control.

It has been proven in [27] that the resistive term of these high frequency impedances, known as the transient resistance, is also relevant in the high frequency response of a permanent magnet machine. This term is a measure of the stator resistance and also the induced currents in the rotor magnets and laminations and a profile of this can also be used to track rotor position.

2.2.2.1 Temperature estimation using HF-injection

One of the sensorless control methods is adapted in [28] to give an estimate of rotor temperature based on the temperature dependant transient resistance calculations derived in [27]. The theory behind this method begins with a high frequency model of the machine (1).

$$v^s_{dq\_hf} = Z^s_{dq} . i^s_{dq\_hf} \quad \textbf{(1)}$$

$$Z^s_{dq} = \sum R + j\omega_c \sum L \quad \textbf{(2)}$$

$$\sum R = R_s + R_r \quad \textbf{(3)}$$

In this model, Z^s_{dq} is the high frequency impedance of the machine, made up of an inductance component $\sum L$ and a resistive component $\sum R$ (2). Both

are made up then of a stator and rotor component defined by the subscripts S and R respectively (3). It is shown in [27] that the resistive terms are temperature dependant, as is the magnetic field created by the permanent magnets as discussed in previous sections.

$$R(T) = R_0(1 + \alpha_{cu}.\Delta T) \quad \textbf{(4)}$$

Where α_{cu} is the resistive thermal coefficient of copper in the case of stator resistance, the magnet for the rotor and T is the stator or rotor temperature.

The inductive term also holds temperature dependant information as this is related to the magnetic field strength produced by the magnets which itself varies with temperature.

$$B(T) = B_{r_0}\big(1 + \Delta T.\alpha_B(T)\big) \quad \textbf{(5)}$$

With B_{r_0} being the residual flux density of the magnet at ambient and α_B is the PM magnetic field thermal coefficient. It can be seen that this relationship is non-linear, making the inductance term more complex to work with. For this reason the resistive term has been used in [28].

Taking the real term from (2) and substituting for the temperature dependent stator and rotor resistances gives an expression which can be rearranged to give the rotor temperature (6).

$$T_r = T_0 + \frac{\sum R_{(T_s,T_r)} - R_{r(T_0)} - R_{s(T_0)}[1 + \alpha_{cu}(T_0 - T_s)]}{R_{r(T_0)}\alpha_{mag}} \quad \textbf{(6)}$$

Rearranging and taking the real part of (1) will give a value for $\sum R_{(T_s,T_r)}$. The stator resistance must be measured with the rotor removed from the

machine at ambient temperature and the result recorded for use in (6), and the rotor resistance can then be estimated by measuring the total resistance and subtracting that of the stator.

This method requires a high frequency excitation, either rotating or pulsating (a rotating injection is demonstrated in [28]). The selection of this excitation, as with sensorless control, is a trade-off between estimate accuracy and the impact on machine performance. A larger amplitude signal is preferable to extract the most information from the machine and to maximise signal to noise ratios. The impact of this however is increased audible noise and possible torque oscillations and/or extra induced losses.

The carrier frequency is also important; it must be high enough to not interfere with the machines current controllers or the fundamental performance but low enough so that the inductive term of the impedance doesn't dominate too much.

2.2.2.2 Temperature Estimation using Test Pulses

Another method is first presented in [29]; this method uses test pulses which exploit the saturation level of the d-axis of a permanent magnet machine in order to extract the field strength of the magnet at the time of the test.

The implementation of the method proposed by Ganchev et al requires accurate knowledge of the rotor position. The aim is to put a very large voltage pulse on the d-axis of the machine and in order to maximise both the accuracy and magnitude of this pulse it is sensible to choose an angle which is a multiple of 60°. This is where the d-axis is aligned with one of the

6 active space vectors and as such the demanded pulse can be applied using just one switching state as shown in Figure 7.

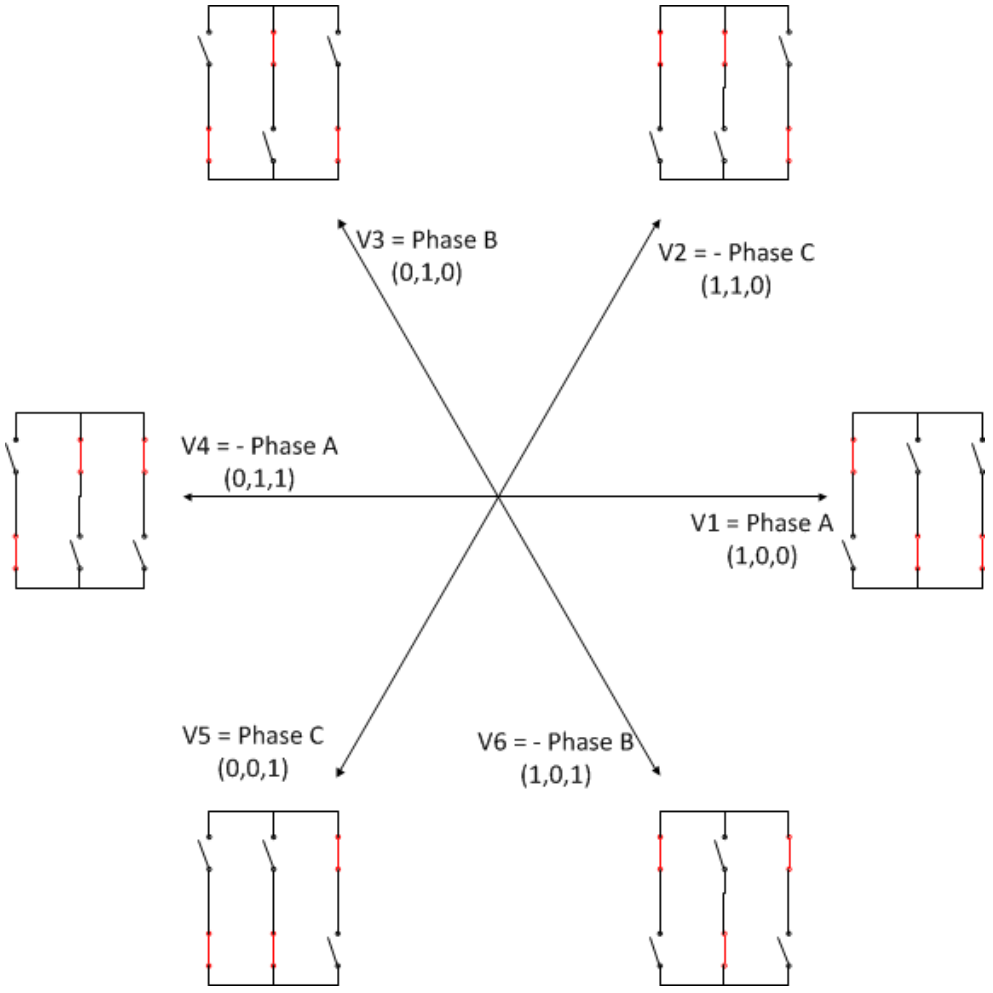

Figure 7: Test pulse switching states

The next step is to oversample the current response to this pulse, enabling the calculation of $\frac{di_d}{dt}$, which given knowledge of the applied voltage and when neglecting stator resistance and cross-coupling will give a direct measure of the d-axis incremental inductance of the machine (7).

$$L_d{}' = \frac{v_d}{\left(\frac{di_d}{dt}\right)} \quad \textbf{(7)}$$

The incremental inductance depends on the level of saturation within the machine which itself is a very non-linear function of the d-axis current and the magnetic field set up by the magnets. The former is known due to oversampling during the voltage pulse and the latter is a temperature dependant parameter of the magnetic material.

If a commissioning phase is carried out for each machine design, a look-up table (LUT) can be created to show the relationship between $\frac{di_d}{dt}$ and the magnet temperature allowing for the saturating effects of the absolute level of d-axis current. This enables a temperature estimate to be obtained in operation without relying on the knowledge of machine parameters.

In practice, the difficulty lies in applying and sampling the test pulse. It requires a supervisory controller to monitor and predict when the rotor angle will cross one of the measurement angles. It must then calculate when within the PWM cycle this will occur. Once the exact pulse required has been calculated then the standard vector control must be paused and a new modulation scheme implemented for the test PWM cycle.

This requires a non-standard PWM system to allow a single phase to be switched with a non-symmetric pulse and also the ADCs to be sampled rapidly for the duration of the pulse. This implementation is very demanding, possibly requiring a change in DSP/FPGA peripherals and potentially additional hardware to enable the precise sampling of the current channels.

2.2.3 Temperature Estimation by Parameter Monitoring

There are two basic theories behind all temperature estimation. One is to have a thermal model of the machine and populate this with thermal resistances and capacitances to give an estimate at different loads given estimated loss inputs and in some cases temperature measurement points using information from thermocouples within the machine. The second is to try to extract information about machine parameters and match this against the expected parameter values for different temperatures. The best fit is then the temperature estimate.

This can be done for various parameters, the previous section looked at exploiting variations in the high frequency impedances caused by induced currents or reduced air gap flux density. As discussed in that section, to extract this information requires an excitation of some form, be it high frequency sinusoidal injection or a modified PWM pattern. This is not desirable; this section will only discuss methods of parameter based temperature estimation using the fundamental response of the machine.

2.2.3.1 Thermal Model Based Magnet Temperature Estimation

Thermal models can be created of a system to make the thermal circuit analogous to that of an electrical circuit. As with an electrical circuit this can be of varying complexity ranging from a steady state model of 2 resistances up to an extremely complex model of a machine geometry taking into account all interfaces and conduction mediums.

Each circuit parameter has to be given a value, either the thermal resistance or capacitance. These values must be calculated from known thermal coefficients and the components geometry. Accurate estimation of these

parameters is very difficult and often requires several iterations through experimentation or finite element modelling to fine tune the system model.

The authors of [30] propose a very simple model, reducing the system to 2 nodes. They are able to do this because of the inclusion of thermal measurement of the stator core in operation and so can keep this point as the input to their model avoiding the need to simulate transfer to the cooling circuit. The parameters for the model are then determined experimentally by running the machine through a commissioning process. This process is carried out once per machine design providing each machine is produced identically and the placement of the stator core measurement is also the same for each machine.

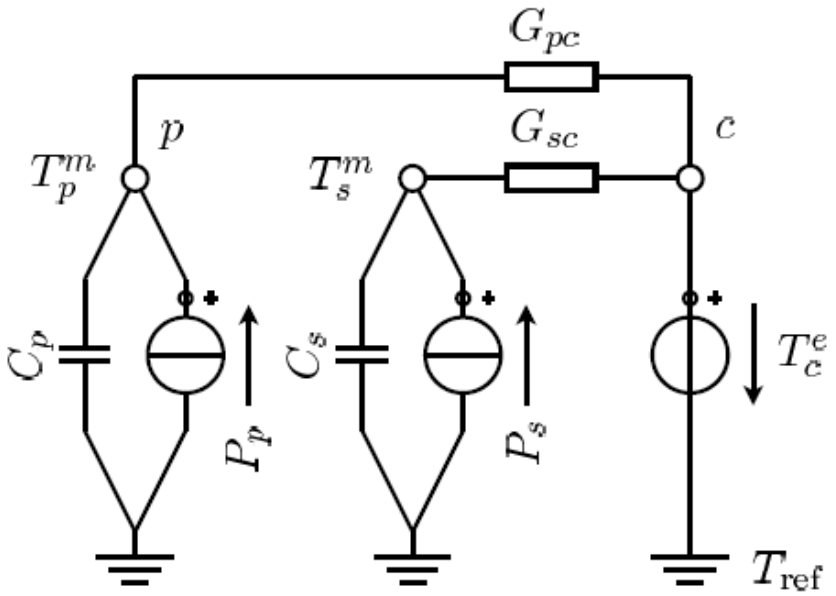

Figure 8: Proposed thermal model with two thermal nodes, i.e., permanent magnets p, stator winding s; the stator core temperature is an input quantity to the model [23]

The other sources for the thermal model are the losses, which must be estimated using loss models in the case of copper losses (P_s) or look-up tables based referencing machine current levels and operating speed for iron losses (P_p). This method then gives an estimate of temperature of the stator windings and of the permanent magnets which match the measured values within +/- 5°C during operation.

This method however assumes a constant average temperature across the winding and magnet geometry and does not account for hotspots. The error is also greatest during transient periods, which is when temperatures are most likely to change quickly and go to dangerous levels.

More detailed models are presented in [31] and [32]. These models offer estimates at more points within the machine geometry but in order to do this they require the calculation of more detailed thermal resistances and capacitances for example the magnet to rotor core interface amongst others must be defined. These models also require the more localised calculation of losses. In [30] there were only two loss inputs to calculate as all iron and magnet losses were input to one node and all copper losses to another. However in more detailed models the iron losses must be broken down into each component of the machine geometry and input to the correct nodes.

A steady state error compared to a finite element model of below 7°C is demonstrated in [32]; however transient performance is not discussed. The authors of [31] use the thermal model as an input to a look-up table which gives explicit limits and deratings for field weakening operation to ensure that the machine is working at a safe operating point for the magnets.

The computing effort required for a complex model can be quite intense and to parameterise the models will involve accurate finite element analysis or detail experimental investigation to give confidence in the estimates. Another issue with the thermal models is their lack of accuracy under transient conditions, when temperatures can be most erratic. However, once a model is satisfactorily developed and tuned then it will work for all machines of the same design without the need for calibration.

2.2.3.2 Temperature Estimation by Rotor Flux Observation

The rotor flux of a PM machine is depends on the size, position and state of the magnets on or in the rotor. For a given machine, the state of the magnet is the only variable parameter and this state will change based on the temperature or damage to the magnet. Therefore the rotor flux contains information about the temperature and condition of the magnets.

In [33] this relationship is investigated by use of a fourth order extended Kalman filter. The resulting rotor flux is then analysed to give an indicator of magnet demagnetisation. The author begins with the standard dynamic machine equations in the rotating reference frame.

$$v_d = Ri_d + L_d \frac{di_d}{dt} - \omega L_q i_q \quad \textbf{(8)}$$

$$v_q = Ri_q + L_q \frac{di_q}{dt} + \omega L_d i_d + \omega \varphi_r \quad \textbf{(9)}$$

Then to allow for a non-sinusoidal flux density the rotor flux linkage φ_r is separated into its d and q axis components. This means (8) and (9) can be rewritten as (10) and (11).

$$v_d = Ri_d + L_d\frac{di_d}{dt} + \frac{d\varphi_{rd}}{dt} - \omega L_q i_q - \omega\varphi_{rq} \quad \textbf{(10)}$$

$$v_q = Ri_q + L_q\frac{di_q}{dt} + \frac{d\varphi_{rq}}{dt} + \omega L_d i_d + \omega\varphi_{rd} \quad \textbf{(11)}$$

If it is assumed that the rotor flux linkage is constant for short time periods, and the equations are rearranged then the set of state equations (12) - (15) can be obtained.

$$\frac{di_d}{dt} = \frac{v_d}{L_d} - \frac{R}{L_d}i_d + \omega\frac{L_q}{L_d}i_q + \omega\frac{\varphi_{rq}}{L_d} \quad \textbf{(12)}$$

$$\frac{di_q}{dt} = \frac{v_q}{L_q} - \frac{R}{L_q}i_q - \omega\frac{L_d}{L_q}i_d - \omega\frac{\varphi_{rd}}{L_q} \quad \textbf{(13)}$$

$$\frac{d\varphi_{rd}}{dt} = 0 \quad \textbf{(14)}$$

$$\frac{d\varphi_{rq}}{dt} = 0 \quad \textbf{(15)}$$

These equations are then evaluated using the extended Kalman filters and the rotor flux linkage information is extracted. This model is still dependant on inductance and resistance values and so is susceptible to variations in these parameters.

In order to then estimate the temperature the flux linkage and loading conditions could be fed into a predetermined look up table containing the expected flux linkage at a certain loading for a range of temperatures and so giving an estimate of magnet temperature.

2.2.4 Conclusions

Knowledge of magnet temperatures is an extremely useful piece of information when controlling a permanent magnet machine, especially when the machine is to be operated in the flux weakening region.

In operation it is clear that a direct measurement is impractical. A lot of the methods needed to extract the temperature from the rotating shaft can be expensive, unreliable and require extra maintenance so increasing the lifetime costs of the machine. It is for these reasons that direct measurement is only an option for calibration and not for use in a final commercial product for automotive applications.

The remaining options all have their own positive and negative points. A thermal model can give a very good estimate in steady state conditions given accurate knowledge of the thermal resistances of the components within the thermal circuit or an extensive calibration scheme producing a large look up table. The models are however susceptible to error given unknown initial conditions or in some cases a cooling failure or other anomaly within the machine. A thermal network model is not exceptionally difficult to implement however and is worth consideration.

The methods involving some form of enhanced excitation do arguably offer the most reliable estimate across the operating range. The obvious downfall for these techniques is the added complexity to the machine excitation. Given the potential for a rotating sinusoidal injection to be implemented for initial rotor position detection, it does seem sensible to investigate the extraction of magnet temperature information using the technique presented in [28] using the same current responses at low and zero speed.

This could give the initial conditions for a thermal network or other integrator based model.

The method likely to be preferred for most of the operating range is one similar to that presented in [33]. This requires work to be carried out to obtain a temperature estimate from a flux or back-emf estimator as stated above, but this work is possible and the potential is for a very reliable estimation. Especially given the addition of a stator resistance estimate based on the accurate knowledge of the winding temperatures from embedded thermocouples. This model based approach also mirrors the high speed position estimation and so seems a sensible approach.

2.3 Sensorless Rotor Position Measurement

The idea of implementing vector controlled electrical drives without the need for position or speed sensors has been extensively researched. The resulting techniques can be categorised into two main groups. The first are based on extracting information from the machine about inherent saliencies which can then be exploited to ascertain the rotor position. The second group is made up of techniques rely on observers or machine models in order to estimate the rotor speed and position. This report will look at examples from both groups, going on to describe a complete sensorless control scheme for IPM machines in more detail.

2.3.1 Saliency Based Sensorless Control

The methods which rely on saliency tracking all have some form of modification to the exciting signals; be it the addition of a high frequency signal or a modification of the fundamental PWM wave. This means that

these techniques lend themselves to low and zero speed operation to allow easy separation of the exciting signals from the fundamental electrical machine frequency [34] [35].

2.3.1.1 The Principle of Saliency

In order to understand the control methods it is important to know the principle of saliency. The simplest definition is that a machines saliency is the variation in the rotor impedance seen when referring this to the stator as the rotor turns. This can be caused by air gap variations, material properties or material saturation. In the case of an interior permanent magnet machine the dominant saliency is caused by the magnets buried within the rotor; this effectively extends the air gap along the axis where the magnet is located due to the material having a relative permeability near to 1 (Figure 9).

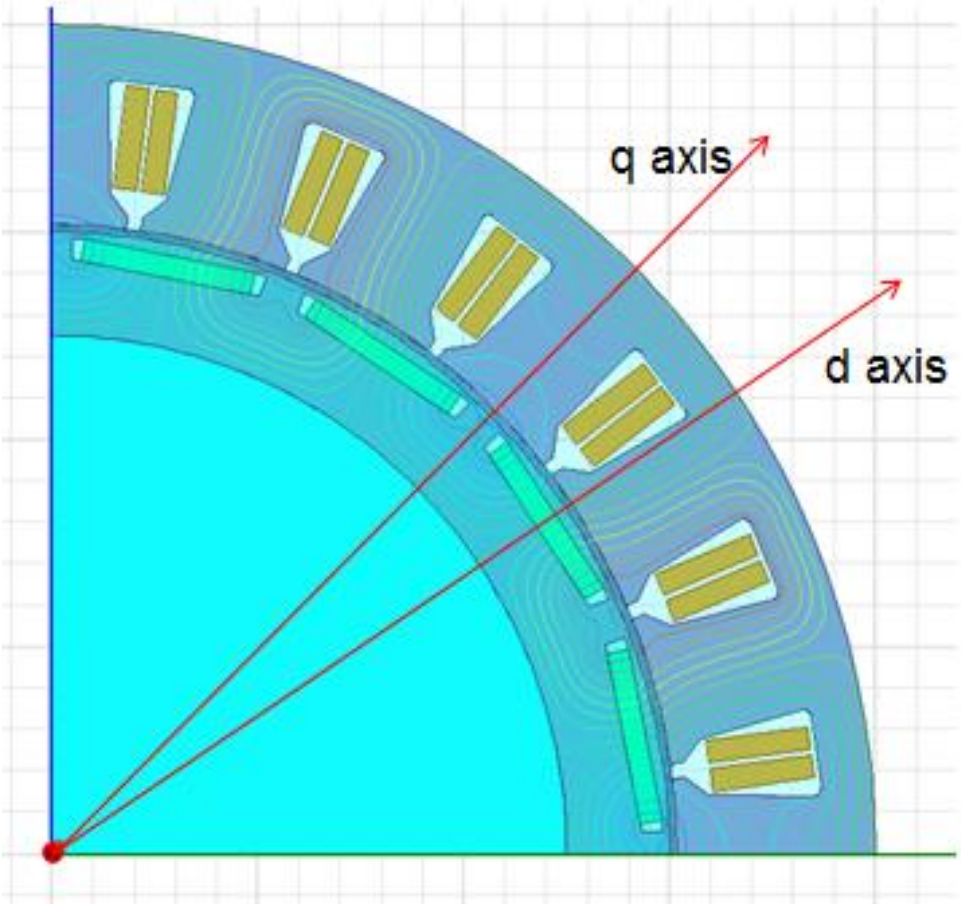

Figure 9: Buried PM machine showing d and q axis. Effective air gap extension visible along d-axis

The variation in the air gap will mean that the inductance along the d-axis is less than that along the q-axis; this variation is measurable from the machine terminals as the rotor turns. For the case of an IPM machine the dominant saliency, caused by the buried magnets, occurs at twice the fundamental electrical frequency. Equation (16) shows the matrix of inductances in the αβ frame for an interior permanent magnet machine.

$$L_{\alpha\beta} = \begin{bmatrix} L - \Delta L \cos 2\theta_e & -\Delta L \sin 2\theta_e \\ -\Delta L \sin 2\theta_e & L + \Delta L \cos 2\theta_e \end{bmatrix} \quad \textbf{(16)}$$

This means that the angle between the poles can be tracked however whether the pole is a north or south is still unknown – this means an initial position scheme is necessary for a saliency tracking sensorless control system.

2.3.1.2 Saliency Extraction using Fundamental PWM Excitations

A machine saliency manifests as a variation in the machine inductance; which can be measured by applying a voltage step and measuring the current response as can be seen from equation (17).

$$V_s = L\frac{di}{dt} \quad \textbf{(17)}$$

As part of a standard PWM excitation scheme thousands of these step voltage changes are applied each second and one technique is to use these steps to calculate the inductance and so track the variation around the machine.

The principle is extremely simple and reliable; however the implementation brings about several challenges.

2.3.1.2.1 Current Derivative Sampling

Assuming that V_s is maintained fixed and stable then equation (17) shows that the derivative of the current is directly proportional to the inductance parameter containing rotor position information as described above. Most industrial or automotive power electronic systems would not measure the derivative of current as standard owing to the fact that it is not a required

variable for standard control techniques. This means that either an extra sensor must be added or a modification must be made to the sampling to allow the derivative to be calculated by sampling the current immediately before the voltage step and then a defined time afterwards and dividing by this time. The challenge here is that several samples must be taken on all phases at precise instants within each PWM cycle; usually requiring a change to FPGA or DSP peripheral programming or design.

2.3.1.2.2 Minimum Pulse Width

The second challenge to overcome is that of parasitic inductance and capacitances along the transmission line. These cause the current to 'ring' immediately after a step voltage is applied as can be seen in Figure 10. The problem this causes is an extension of the time between samples before the derivative can be accurately calculated as the ringing needs to subside (in the order of 5μs depending on machine and parasitic parameters).

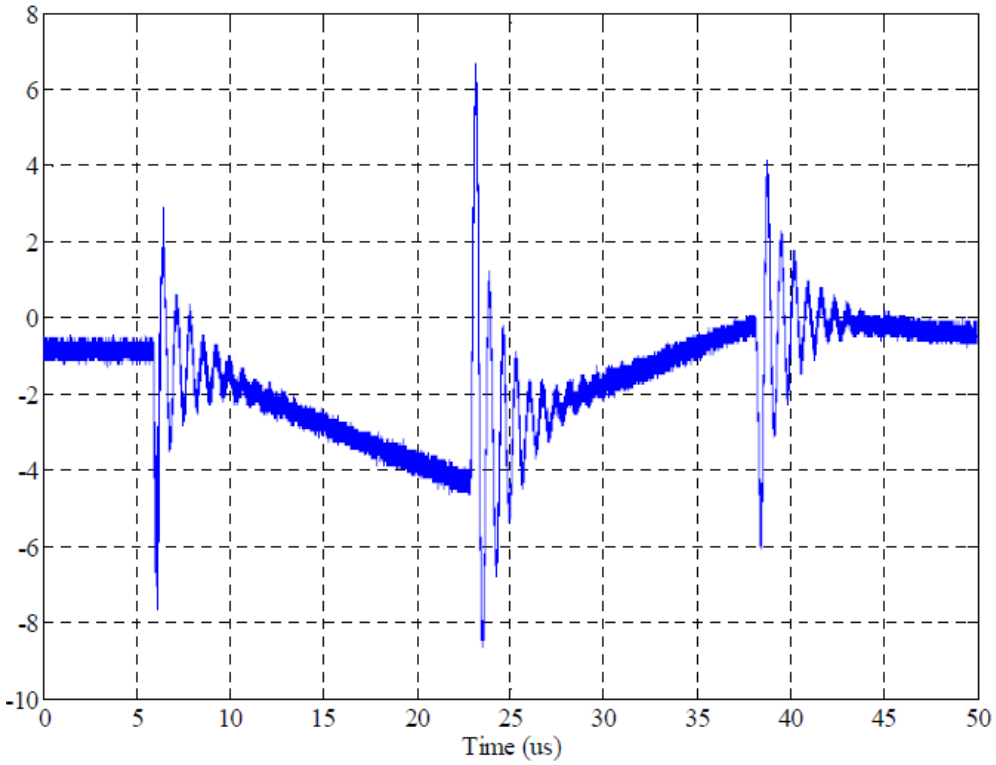

Figure 10: Current waveform during PWM transients

Sometimes the time a certain vector is applied is too short to allow this ringing to subside sufficiently to take a reading. These pulses must then be extended and compensated for by applying a voltage in the opposite direction later at another point in the PWM period in order to bring the mean effect back to the demanded values and not to affect the fundamental vector control. Care must also be taken to account for the effects of dead time when applying the vectors and sampling the waveforms.

2.3.1.2.3 Creating the Position Signals

In each PWM cycle there will be two derivative measurements from active switching vectors available; which two depends upon the angle of the

requested voltage vector. This voltage vector will lie within one of 6 60° sectors, and the equations required to extract a position signal from the derivatives of each sector can be found in Figure 11. Once extracted the signals P_a, P_b and P_c can be transformed into the static αβ frame using the standard equations. The angle between P_α and P_β will then yield the saliency position, and from this the speed can also be calculated. More detailed information and calculations for this technique can be found in [36].

Sampled Vectors	p_a	p_b	p_c
V_1,V_0	$1+c(\frac{di_b^{(1)}}{dt}-\frac{di_b^{(0)}}{dt})$	$-2+c(\frac{di_a^{(1)}}{dt}-\frac{di_a^{(0)}}{dt})$	$-1+c(\frac{di_c^{(1)}}{dt}-\frac{di_c^{(0)}}{dt})$
V_2,V_7	$-2-c(\frac{di_c^{(2)}}{dt}-\frac{di_c^{(7)}}{dt})$	$1-c(\frac{di_b^{(2)}}{dt}-\frac{di_b^{(7)}}{dt})$	$1-c(\frac{di_a^{(2)}}{dt}-\frac{di_a^{(7)}}{dt})$
V_3,V_0	$1+c(\frac{di_a^{(3)}}{dt}-\frac{di_a^{(0)}}{dt})$	$1+c(\frac{di_c^{(3)}}{dt}-\frac{di_c^{(0)}}{dt})$	$-2+g(\frac{di_b^{(3)}}{dt}-\frac{di_b^{(0)}}{dt})$
V_4,V_7	$1-c(\frac{di_b^{(4)}}{dt}-\frac{di_b^{(7)}}{dt})$	$-2-c(\frac{di_a^{(4)}}{dt}-\frac{di_a^{(7)}}{dt})$	$1-c(\frac{di_c^{(4)}}{dt}-\frac{di_c^{(7)}}{dt})$
V_5,V_0	$-2-c(\frac{di_c^{(5)}}{dt}-\frac{di_c^{(0)}}{dt})$	$1+c(\frac{di_b^{(5)}}{dt}-\frac{di_b^{(0)}}{dt})$	$1+c(\frac{di_a^{(5)}}{dt}-\frac{di_a^{(0)}}{dt})$
V_6,V_7	$1-c(\frac{di_a^{(6)}}{dt}-\frac{di_a^{(7)}}{dt})$	$1-c(\frac{di_c^{(6)}}{dt}-\frac{di_c^{(7)}}{dt})$	$-2-g(\frac{di_b^{(6)}}{dt}-\frac{di_b^{(7)}}{dt})$

Figure 11: Position signal extraction from a delta wound machine

2.3.1.3 Saliency Extraction using High Frequency Injection

The saliency can also be extracted by a high frequency voltage signal. When this signal is applied at the machine terminals the current response is modulated by the machine impedance. This impedance, dominated by the inductance due to the high frequency, will vary as the machine rotates and

so will have a similar appearance to that of a resolver sin or cos output. Then with some signal processing the speed and position can be found.

The use of a high frequency signal, much higher than the fundamental machine frequency, means that the estimation method can be implemented alongside a standard vector control scheme. The exciting signal can be simply added to the voltage demand prior to the PWM module, and the HF response can be filtered from the currents prior to the frame rotations in order to not affect the current controllers.

2.3.1.3.1 The HF-Response

The response of PM machine to an exciting signal can be seen in equation (18); this shows the exciting voltage is made up of the resistive voltage drop across the stator windings, the inductive response to the change of current and a term proportional to speed and the rotor flux.

$$V_{\alpha\beta} = i_{\alpha\beta}.R_s + L_{\alpha\beta}\frac{di_{\alpha\beta}}{dt} + \omega_r.\varphi_m \quad \textbf{(18)}$$

If the exciting signal ($V_{\alpha\beta}$) is a pair of high frequency sinusoids, as in equation (19), then the current response can be described by equation (20) where $V_{\alpha\beta}$ and ω_i are the injection voltage and frequency. This equation ignores the back-emf term due to the low motor speed and also the resistive term is neglected because the inductive term is so dominant at high frequencies.

$$V_{\alpha\beta} = V_s\begin{pmatrix}\cos\theta_{hf}\\ \sin\theta_{hf}\end{pmatrix} \quad \textbf{(19)}$$

$$\begin{pmatrix} i_{\alpha^{hf}} \\ i_{\beta^{hf}} \end{pmatrix} = \frac{V_{\alpha\beta}}{\omega_i.(L^2 - \Delta L^2)} \begin{bmatrix} L\sin(\omega_i t) + \Delta L \sin(2\theta_e - \omega_i t) \\ -L\cos(\omega_i t) - \Delta L \cos(2\theta_e - \omega_i t) \end{bmatrix} \quad \textbf{(20)}$$

Equation (20) can be separated into a positive (21) and negative (22) sequence current. The interesting position information clearly appears in the negative sequence.

$$i_{pos} = \frac{V_{\alpha\beta} L}{\omega_i (L^2 - \Delta L^2)} \begin{bmatrix} \sin(\omega_i t) \\ \cos(\omega_i t) \end{bmatrix} \quad \textbf{(21)}$$

$$i_{neg} = \frac{V_{\alpha\beta} \Delta L}{\omega_i (L^2 - \Delta L^2)} \begin{bmatrix} \sin(2\theta_e - \omega_i t) \\ \cos(2\theta_e - \omega_i t) \end{bmatrix} \quad \textbf{(22)}$$

Looking at the amplitude term of the equations also highlights an interesting engineering trade-off; the amplitude of the signal is proportional to the amplitude of the injected voltage and inversely proportional to the frequency. This means that to get a clear position signal the injected amplitude should be high; however this would clearly mean more noise and losses in the machine. It also shows that ideally the injection frequency should be low, but low frequencies will be more difficult to filter from the fundamental current waveform and can interfere with current controllers. A low frequency would also bring into question the assumption that the inductive term is dominant over the resistance and so could complicate the estimation algorithm itself. It can also be seen that the amplitude will go to zero for a non-salient machine, or in fact a salient machine driven into saturation where $L_d = L_q$.

2.3.1.3.2 Extracting the Position Signal

Processing the current response in order to extract the rotor position is where most of the complexity lies in implementing an injection based sensorless scheme. This is the area where there is the largest variety of techniques in literature depending on the test machine and control circuit as well as the choices of the individual implementing the design.

The main principle is to isolate the negative sequence of the HF current response (22) by filtering the fundamental currents and the positive sequence term. Once the negative sequence is isolated then this can be tracked by using one of a variety of demodulation techniques. One possible implementation of this can be seen in Figure 12.

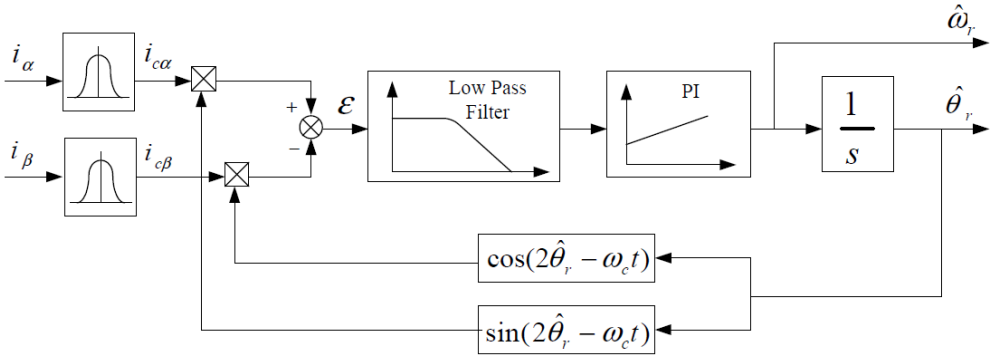

Figure 12: Diagram of a position and speed demodulation system

The HF response is isolated by use of a band pass filter working on the measured currents in the stationary αβ frame. The next step is to take the cross product of the HF response with a signal recreated to have the same phase as the HF response. This is done by using the estimated rotor position and the actual injection signal phase. The result of this cross product is the

angular error between the measured negative sequence current, containing the actual rotor position information, and the signal recreated using the estimated rotor position. Therefore this error is effectively the error between the actual rotor position and the estimate used in the phase recreation. A low pass filter removes noise from the error, giving a more stable speed estimate and a PI controller will ensure that the speed has zero steady state error. The integral of the speed forms the rotor position estimate which is fed back into the cross product. The whole system operates as a phase-locked loop would and with well-tuned gains and filters will provide a stable and accurate speed and position estimate.

An improvement can be made to this demodulation process by incorporating some knowledge of the mechanical system and the power output of the machine in a mechanical observer. In Figure 13 a mechanical observer monitors the developed torque from the machine and using the inertia can then give an estimate of the acceleration, speed and position of the rotor as the machine operates. Here the error term from the cross-product feeds into this observer through a PID controller, acting as a fine tuner for the overall observer and ensuring that the rotor position is accurate.

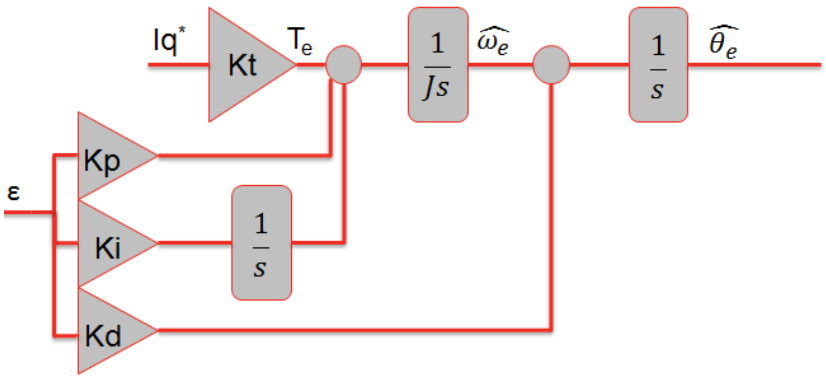

Figure 13: Mechanical observer with position error feedback tuning

This demodulation technique offers improved dynamic performance by taking into account the produced torque and system inertia during operation. It does however require knowledge of these parameters which can both vary during the operation of the drive. The PID controller will work to cope with these variations, and the system does still operate well even with poor knowledge of the inertia and applied torque.

2.3.2 Model Based Sensorless Control

Model based control methods tend to operate by estimating the back-emf component of the machine response. This is quite intuitive, as the back–emf is created by the rotor flux crossing the winding coils, therefore knowledge of the location of the peak emf will give the location of the rotor magnets. The reliance on the back-emf provides one of the weaknesses of the method, estimation is impossible at low and zero speeds, where the back-emf is low.

This section will focus on the model reference adaptive system (MRAS) shown in Figure 14. This is where two different models give an estimate of the stator flux vector, these estimates are compared and an error term is calculated which is then fed back to the adaptive model with some adjustment mechanism ensuring this error is controlled to zero. Each model will be explained, followed by the adjustment mechanism.

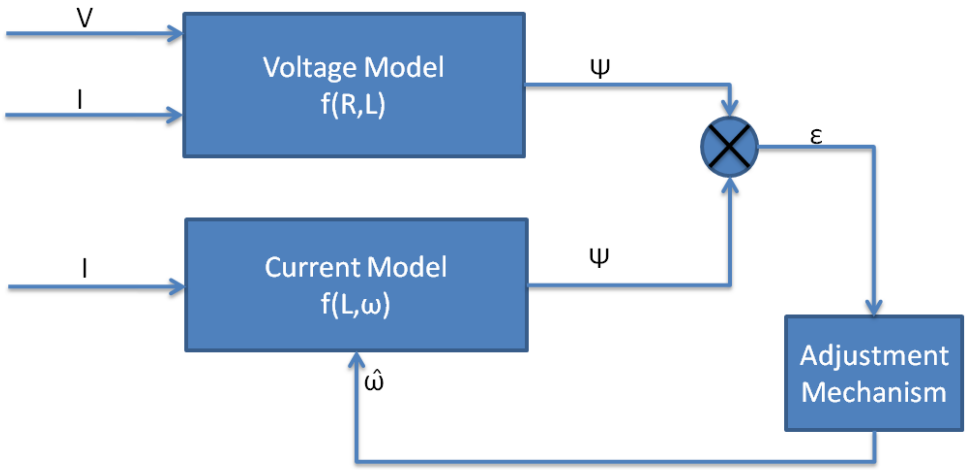

Figure 14: MRAS system block diagram

2.3.2.1 Reference Model

The reference model will give an estimate of the stator flux independently of rotor position, so is not susceptible to error in the position estimation, it is however susceptible to other inaccuracies. The basis for the model is the integral of the stator voltage in the αβ stationary frame (23). It is possible to obtain a very rudimentary position estimate by simply taking the arc tan of this flux vector; but the calculation is reliant on accurate knowledge of R_s which varies during operation, and is also subject to integrator drift meaning that the estimate would be quite inaccurate.

$$\widehat{\varphi_{s_{\alpha\beta}}} = \int (V_{\alpha\beta} - i_{\alpha\beta}.R_s)\, dt \qquad \textbf{(23)}$$

2.3.2.2 Adaptive Model

The second model must rely on one of the required outputs, so in this case it is to be calculated in the rotor reference frame and therefore needs the

estimated rotor position in order to transform the stator current and voltage values to their dq equivalents and then the reverse transform for the flux estimate to be compared with the reference model.

$$\widehat{\varphi_{s_{\alpha\beta}}} = \left(\varphi_m + L_d i_d + jL_q i_q\right).e^{j\widehat{\theta_r}} \quad \textbf{(24)}$$

The adaptive model also relies on machine parameters which can vary within operation, on this occasion it is the d and q inductances. The closed loop system however is still able to provide an accurate estimate with a quite large error in Ld and Lq.

2.3.2.3 Adjustment Mechanism

The adjustment mechanism can take many forms with varying complexity. The theory is very similar to that described in Figure 12 and Figure 13, the only difference being that the controller or observer is being driven by the angular error between the two stator flux vector estimates. For the ease of implementation and code repetition, if designing a complete sensorless control scheme it is logical to use the same implementation for both injection and model based control.

2.4 Conclusion

This chapter has reviewed a particular piece of legislation which is driving a need for intelligent fault monitoring, detection and diagnostic techniques within the automotive industry. A comprehensive review of this standard has shown how such techniques must be designed into a product, driven by an analysis of failure modes, in order to mitigate unsafe system reactions which could put public road users at risk.

The second part of the chapter has then focussed on a particular part of the electric machine; the permanent magnets. It has looked at current methods to monitor the condition of these magnets in order to react to potential faults and hazards caused by over temperature or demagnetisation. Current literature can be divided into three main categories; the first reliant on thermal measurements which are difficult to achieve in a compact and cost restricted system, the second set is focussed on various thermal models requiring knowledge of initial conditions or settling times to ensure accuracy and the third utilise various injection methods to interrogate the magnetic circuit within the machine in order to extract magnet information. These techniques all suffer from a need for expensive and complex sensing technologies, high processing demands or high frequency excitations; all undesirable characteristics when designing an automotive system.

The final part of this chapter reviewed current literature regarding sensorless control techniques. There is an overwhelming amount of material and research available in this field; however there still remains a huge challenge regarding rotor position estimation at low and zero speeds in an application where electromagnetic compatibility is so stringently regulated. Some authors have specifically looked to reduce audible noise [37] [38] however these techniques do not address the wider spectrum and high frequency harmonics which could cause issues in emissions at much higher frequencies.

Therefore; work is still required in these areas in order to develop algorithms which are fully compliant with the automotive industry demands. The remainder of this thesis will go on to further investigate the issues around sensorless control; creating a tool which could be used to assess the impact

of transient excitation schemes on motor phase currents in simulation and then later implementing a scheme which may be acceptable at power up in an automotive system to confirm the correct operation of a traditional position sensor.

A novel solution to the magnet condition monitoring question will be developed. This is an algorithm which can provide information about the magnets without expensive components or processing overhead; this technique will be derived and proven in simulation and experimentally.

3 Simulation of a Sensorless Control System Based on Fundamental PWM Transient Excitations

A simulation of a sensorless control scheme using the fundamental PWM transients is described in this section. The aim is to create a model which acts as closely to a real DSP controlled drive system as possible whilst ignoring the power converter non-linearity. The model is created in MATLAB/Simulink and is based around three C-Script blocks. The first contains a space vector pulse width modulation (SVPWM) generation algorithm incorporating a minimum pulse width and compensation scheme similar to those documented in [39] [40] [41]. The second is designed to simulate a current derivative sensor. The third is used to extract the position signals from the current derivatives. The remainder of the model is a standard vector control loop controlling a permanent magnet synchronous machine. The model controls the direct axis current (i_d) to zero and so does not simulate any field weakening or maximum torque per amp (MTPA) scheme. Another scheme could easily be introduced if required using standard vector control modelling techniques as the SVPWM and position estimation blocks are independent of the control implemented around them. Figure 15 shows a block diagram of the simulated control system.

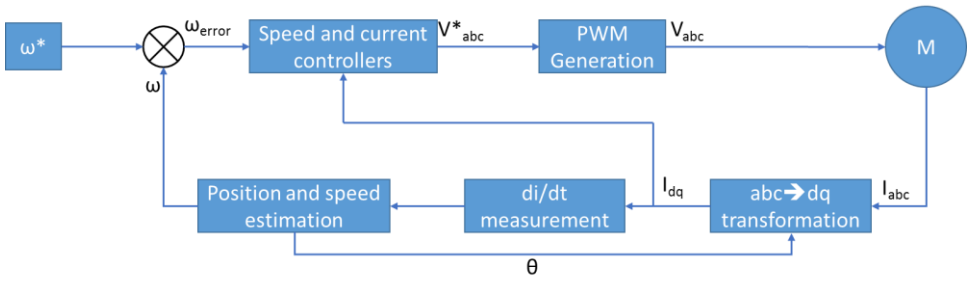

Figure 15: Block diagram of the simulated control system

The speed and current controllers are based on standard control theory, with a current or torque loop inside a speed loop. There are independent PI controllers for i_q and i_d and as stated above i_d is controlled to zero. The assumption made that i_q is proportional to the generated torque. This assumption means that the output of the speed controller can be used as an i_q demand given knowledge of the motor torque constant (k_t).

The final block in the feedback path in Figure 15 is actually made up of two independent blocks. It contains the position estimation C-script block described above and also a mechanical observer and controller to ensure an accurate position estimate as described in [36].

3.1 SVPWM Generation Block

This block has been designed to simply take in a three phase voltage (v_{abc}) demand and output the actual terminal voltages seen across the machine windings. By effectively incorporating the power electronics into the SVPWM generation this method does not model the effects of dead time, DC-Link voltage (V_{dc}) variations and any non-linearity associated with the inverter switching.

The SVPWM generation is calculated in real time, by firstly transforming the three phase demands V_{abc} into a static two phase demand $V_{\alpha\beta}$ .This can be converted to a demanded angle and amplitude, effectively a voltage vector which fits on the space vector plane.

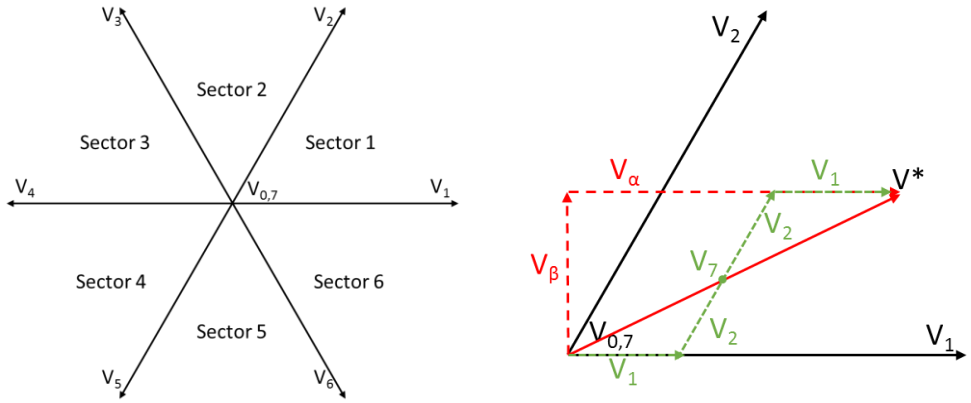

Figure 16: Left: The space vector plane with all vectors and sectors highlighted. Right: A voltage demand in sector 1 and the vector sequence applied to achieve it

The plane is made up of six 60° sectors separated by six active vectors (V_1 to V_6), and two zero vectors (V_0 and V_7) as shown in Figure 16. Any voltage demand can be made up of two active vectors and by appropriately placing the two zero vectors a recognizable PWM pattern can be achieved which will give the demanded voltage vector. Figure 17 shows the approximate PWM waveform for the demand shown in Figure 16.

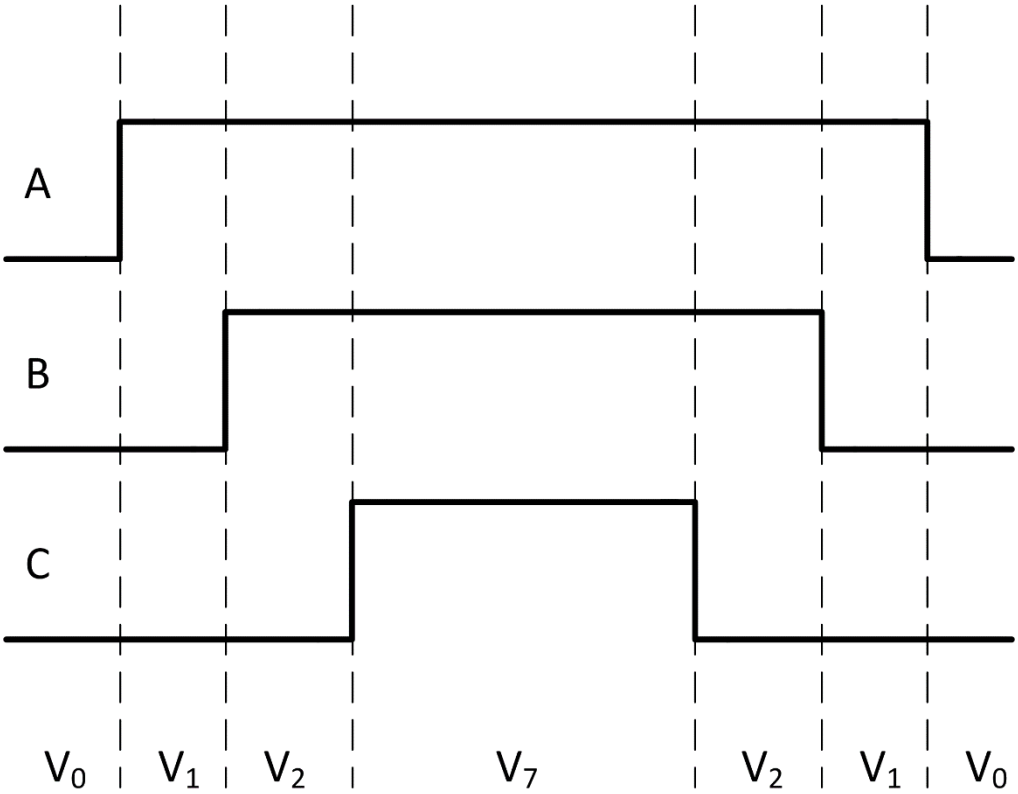

Figure 17: A symmetrical PWM waveform constructed from active and zero vectors

These voltages are then applied to the terminals of a SimPower interior permanent magnet machine using controlled voltage source blocks in order to obtain the required mechanical response.

This block in combination with the speed and torque control loops and a current and position sensing feedback loop would make a standard vector controlled system; where this model differs is in the remaining two C-Script blocks which in turn selectively sense current derivatives and using this information calculate the rotor position.

3.2 Derivative Current Sensing

In practical experiments the measurement of current derivatives can be made using a Rogowski coil [42]. This is a reasonably simple device, a wire wound toroid through which a conductor is fed through. The voltage seen across the coil is then proportional to the rate of change of the current flowing in the conductor fed through it. This voltage can be calculated from (25).

$$V_{coil} = \frac{-AN\mu_0 l}{di/dt} \quad \textbf{(25)}$$

Where A is the area of one turn, N is the number of turns, μ_0 is the permeability of free space, l is the length of the winding and d_i/d_t the rate of change of current in the conductor.

This however would be difficult to simulate accurately within Simulink and so it was decided to implement a simpler method. The chosen technique takes two separate samples of the current and divides the difference between them by the time between the samples. In practice this method is difficult to implement due to the required frequency and precise timing of current sampling, however in simulation this can be overcome. Using this simplified method means that the effect of sensor bandwidth can easily be highlighted by changing the time between samples and analysis of this could easily be carried out because of the fact that each block is completely independent of the rest of the simulation.

3.3 Position Estimation

The position estimation block is an implementation of the techniques described in [25], [39], [36], [43] and [44]. It is a standard technique to extract position estimation from current derivatives, carried out in simulation using the third C-Script block. The technique obtains the position by calculating the inductance profile of the machine in real time using the di/dt measurement as shown in chapter 2.

Once the correct equations have been selected, current derivatives sampled and the three phase position signal calculated the final task carried out by this C-Script block is to convert the three phase position information into a two phase αβ resolver signal. This can be processed by a mechanical observer in the final Simulink block to extract the electrical and mechanical position and speed.

3.4 Simulation Results

The final model can simulate a closed loop sensorless control system based on the di/dt method of position estimation. The design of the model means that it can be easily adapted for different machines and even for different vector extension and compensation schemes. Figure 18 shows a speed response to a stepped speed demand from 0 to 30 rad/s followed by a load step in load illustrating the agreement between estimated and real speed and position.

This model could be paired up with a suitable finite element package allowing investigations into the saliency profiles of various IPM designs;

immediately being able to assess effective they would be under a PWM transient excitation scheme.

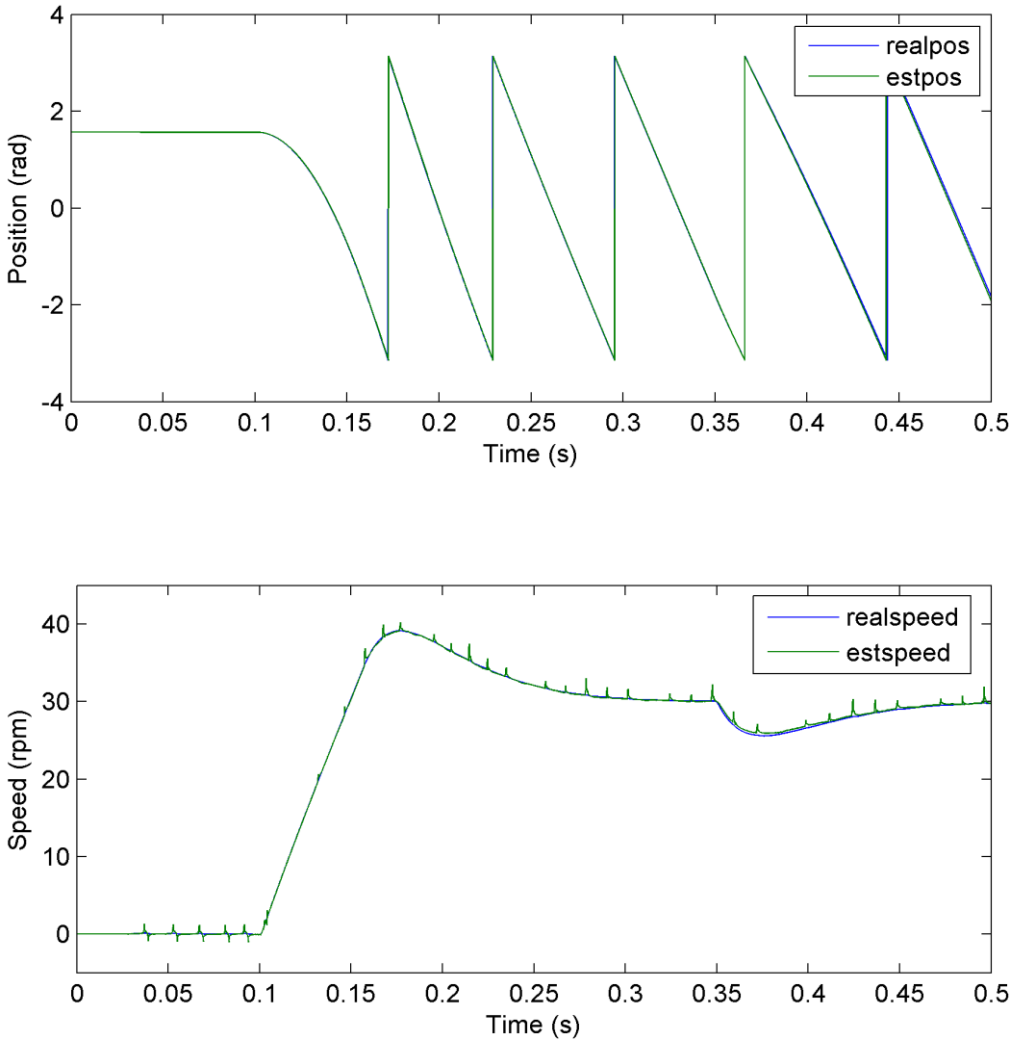

Figure 18: Simulation results showing the actual and estimated position and speed of a machine subjected to a stepped speed demand followed by a load disturbance

3.5 Conclusions

While the techniques simulated above may not be suitable for use in an automotive system due to the additional current disturbance inevitably created by the modification of PWM switching edges, the model developed in this chapter could be used to help further the understanding and development of fundamental PWM transient excitation based sensorless control methods. There is also an area of research into the magnetic design of permanent magnet machines specifically to support sensorless control [45] [46] [47] [48]; this model linked to a suitable finite element package would enable that work to be carried out in simulation and to compare the closed loop performance of systems using several machine topologies before prototyping.

4 Development of an innovative Magnet Condition Monitoring Scheme

This chapter will describe the development of a novel magnet condition monitoring scheme specifically for an interior permanent magnet motor. This scheme does not require any physical measurements of the rotor other than a standard position measurement which is also essential for accurate closed loop control. It also does not require the injection of high frequency signals or modification of the control switching patterns as many of the techniques described earlier in this thesis.

The first part of this chapter describes the theory behind this method; deriving and defining the equations which will be solved in real time to derive a measure of the magnet condition. The chapter will the go on to describe the simulation of this method, demonstrating the robustness to variations in several parameters and external conditions. The implementation of the scheme is then described in chapter 7.

4.1 Derivation of Magnet Condition Monitoring Model

4.1.1 Back-EMF Estimation

The first step to estimating magnet temperature is to derive the machine back-emf. This is basically the voltage across the stator windings induced by the magnet flux linkage. This quantity is not directly measurable while the machine is on load because of the voltage drop across the winding

impedance due to load currents. This is clear when looking at the machine phasor diagram – shown in Figure 19 in motoring mode.

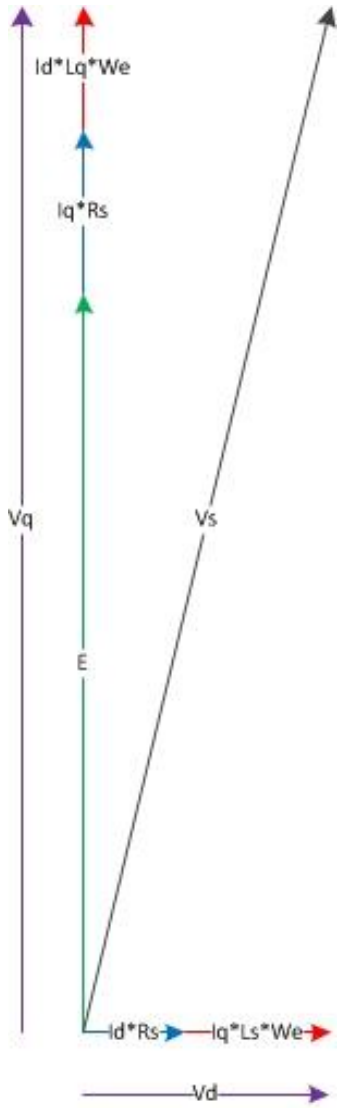

Figure 19: Phasor diagram of a PM synchronous machine

This means that the use of a sensor or the controller demand variable directly is not an option. The steady state voltage equations of a PM machine in the rotating d-q reference frame are given in equations (26) and (27). It can be seen that the back-emf term only appears in the q-axis equation

(27); this can then be extracted by rearranging into equation (28) and solving.

$$V_d = I_d R_s - I_q L_q \omega_e \quad \textbf{(26)}$$

$$V_q = I_q R_s + I_d L_d \omega_e + E\left(K_{emf}, \omega_e\right) \quad \textbf{(27)}$$

$$E = V_q - I_q R_s - I_d L_d \omega_e \quad \textbf{(28)}$$

Isolating the back-emf term requires accurate knowledge of the q-axis current (Iq), the phase resistance (Rs) and the q-axis terminal voltage Vq. The current can be taken from the Iq ref measured values, the terminal voltage can be taken from the Vq reference sent to the PWM module and the resistance can be measured at the machine terminals.

4.1.2 Back-EMF to Temperature

Once an accurate Back-EMF estimate is obtained then extraction of the temperature is possible. The Back-EMF term, in its simplest definition, can be seen in equation (29). This shows the speed constant (K_{emf}) multiplied by the electrical rotational frequency. This shows that the back-emf will vary due to any changes in both the speed constant and the rotational speed. Therefore the back-emf will be divided by the rotational speed to yield the machine constant K_{emf} – this will allow speed independent identification of the temperature.

$$E = K_{emf} \omega_e \quad \textbf{(29)}$$

The final stage is to determine the machine temperature from the speed constant. Theoretically this can be calculated by use of finite element simulations or analytical equations however these methods both make assumptions and linearise certain effects to make the calculations practical. Therefore the preferred method is to create a look-up table or curve fit of this data based on experiments. Gathering this data is relatively simple; the machine can be operated under load, with measurement of the rotor temperature. As the machine heats up through operation the load and control can be removed and the back-emf measured with the machine at rated speed using a dynamometer. This data can be recorded at various temperatures and so a plot of back-emf Vs temperature can be created. Dividing the back-emf value by the rated rotational speed will then give a plot of the speed constant Vs temperature.

4.2 Simulation of Magnet Condition Monitoring Scheme

The implementation of the above method was carried out firstly in simulation which will be described in detail in this chapter. This involved the creation of a temperature dependant machine model within Matlab/Simulink; the creation of this model forms the first section of the chapter. Once this had been created, the temperature observer was then added to the model; described in the second section and the third section presents a series of simulations which were ran to ensure the system worked on an idealised system. Investigation of the robustness to parameter inaccuracy was also investigated and reported within this section. The final section goes on to show the conclusions drawn and the main points

of learning to be carried forward to the physical implementation of the estimation observer.

4.2.1 Temperature Dependant Machine Model

The basic model is current fed, based on the d-q voltage equations (26) + (27). These equations have two temperature dependant parameters, the first is the stator resistance and the second is the speed constant. A separate block was created for the calculation of each of these parameters and fed into the main model; these blocks will be described in their corresponding subsections.

The demands to the main model come in the form of Id and Iq references with ideal control and power supplies assumed. This enables the easy application of various load levels and flux weakening currents. These demands are passed to the main machine model along with the speed, speed constant and temperature dependant resistance. The output is then in the form of the terminal voltages and the rotor position which can be used to transform back to the 3-phase currents and voltages.

4.2.1.1 Resistance Calculation

The windings of the machine are made from a standard copper wire. The resistance of the wire can be calculated quite simply using (30). The change in length and cross section due to temperature is negligible, and so the only thermally sensitive parameter is the resistivity ρ_{cu}. This deviation can be assumed to be linear across the range of interest (-40 to 200°C) and it follows that the change in resistance can also be assumed to be linearly proportional to the temperature of the copper.

$$R_{cu} = \frac{l\rho_{cu}}{\pi r^2} \quad \textbf{(30)}$$

One of the properties given for electrical materials is the thermal coefficient of resistivity; this value shows the percentage change in resistivity per degree centigrade/Kelvin, for copper K_{cu} = 0.003862. Therefore the variation in resistance can be extracted using (31) where R_0 is the initial measured resistance at temperature T_0, K_{cu} is the thermal coefficient of resistivity of copper and $T_{winding}$ is the current winding temperature. This equation is implemented inside the resistance calculation block, receiving the current winding temperature and outputting the revised winding resistance.

$$R_{winding} = R_0\{1 + (T_{winding} - T_0)K_{cu}\} \quad \textbf{(31)}$$

4.2.1.2 K_{emf} Calculation

The calculation of the speed constant is a complicated non-linear equation derived from the machine geometry, material properties, and temperatures. For most situations this can be assumed constant once calculated or measured for the desired operating point of a machine, however these small variations contain vital information about the temperature of the magnets.

In attempting to simplify the relationship certain assumptions can be made; for example high loading conditions will affect the flux linking the magnets and the stator windings due to saturation of the stator iron – therefore reducing the induced voltage and so the speed constant. This can be assumed linear for the range of operation as saturation does not occur in

this machine until extreme overload conditions, which is proven experimentally in the following section.

It can eventually be shown, and experimentally proven, that for the required range of operation of this machine the speed constant has a linear relationship to temperature. This is because the only variant that has a substantial effect on the constant in this range is the magnet residual flux density – a parameter which is directly related to the temperature of the magnet through (32). Where α_{br} is the thermal coefficient of residual flux density.

$$B_r = B_0\{1 + (T_{magnet} - T_0)\alpha_{Br}\} \quad \textbf{(32)}$$

It can therefore be said that the speed constant will have the same relationship with temperature and so the change in speed constant can be calculated using (33).

$$K_{emf} = K_{emf0}\{1 + (T_{magnet} - T_0)\alpha_{Br}\} \quad \textbf{(33)}$$

4.2.2 Magnet Temperature Observer Model

The temperature observer has been implemented in the same Simulink model following the theory described earlier in the chapter. There is a separate parameter file which describes the machine and initial parameters for the temperature dependant terms which can then be called anywhere in the model.

The observer takes the form of two blocks. The first extracts the speed constant; taking in the voltages and currents in the rotating reference frame along with the rotational speed. This block then outputs the estimated back-

emf for observation and also the speed constant to pass forward to the second observer block.

The second observer block then converts the speed constant into a magnet temperature estimate. As previously stated, the analytical link between the speed constant and the rotor constant is very complex, however for the range of operation this relationship can be approximated to a linear equation relying only on the coefficient of residual flux density and one measured initialisation point.

4.2.3 Simulation Results

With the operation of the model confirmed a set of tests can be carried out to gain an understanding of the accuracy and robustness of the observer. Each test will be described in the following sections.

4.2.3.1 Constant Temperature Operation

The first test will confirm that the observer and model are working correctly. With all temperatures fixed the machine is taken through a test schedule where the speed ramps from standstill to rated speed where the load will step to rated current before dropping off and the machine is brought back to standstill. The results are shown in Figure 20; firstly the speed plot, the second plot shows the load current and the back emf estimate from the observer and the final plot shows the temperature estimate against the actual setting of the magnet temperature.

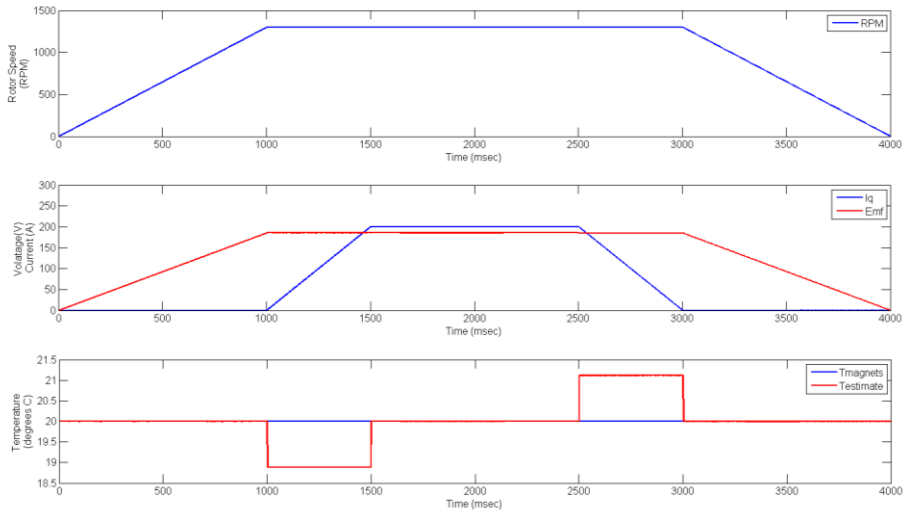

Figure 20: Constant temperature test. Top: Rotor speed, Middle: Measured Iq and Back-EMF Estimate, Bottom: Actual magnet temperature and observer magnet temperature

It is immediately obvious that there is an error in the estimate during the load transient period; this is expected as the current derivative term has been neglected from the observer equations. This is to avoid the need for a differentiator in the real world application due to the additional noise it would bring to the estimation due to fluctuations in the steady state currents.

4.2.3.2 Heat Run Simulation

The aim of this test is to mimic the conditions seen in a standard end of line heat run test. The load and speed are constant rated values but the winding and magnet temperatures are increased. The simulation allows this gradient to be increased to save time, but the model stability and results are still

representative. The winding temperature and the actual and observed magnet temperatures are displayed in Figure 21.

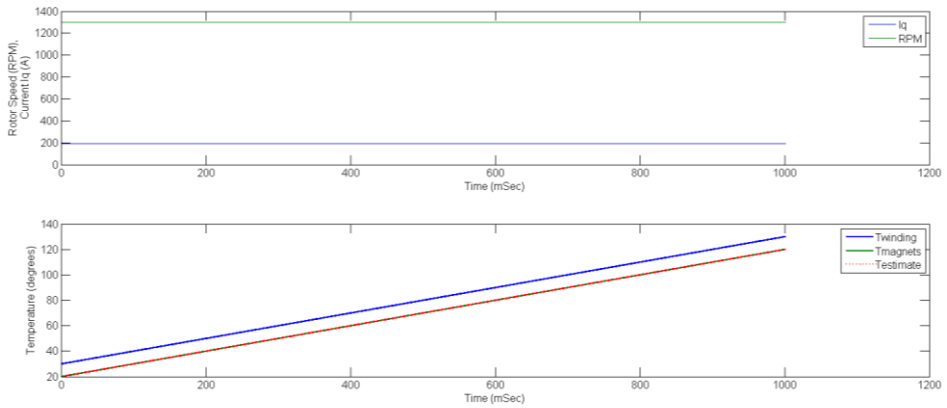

Figure 21: Heat run test. Top: Constant Speed and Load. Bottom: Actual winding temperature, actual magnet temperature and observer magnet temperature.

4.2.3.3 Stator Resistance Sensitivity Test

This test will show the tolerance of the method to the variation in stator resistance which can be seen between machines in production. The R_0 term inside the machine model is varied from that in the observer by +/- 10% of the nominal value and simulated at full load at 90°C magnet temperature and 100°C winding temperature. The error in temperature is plotted against the error in Rs in Figure 22.

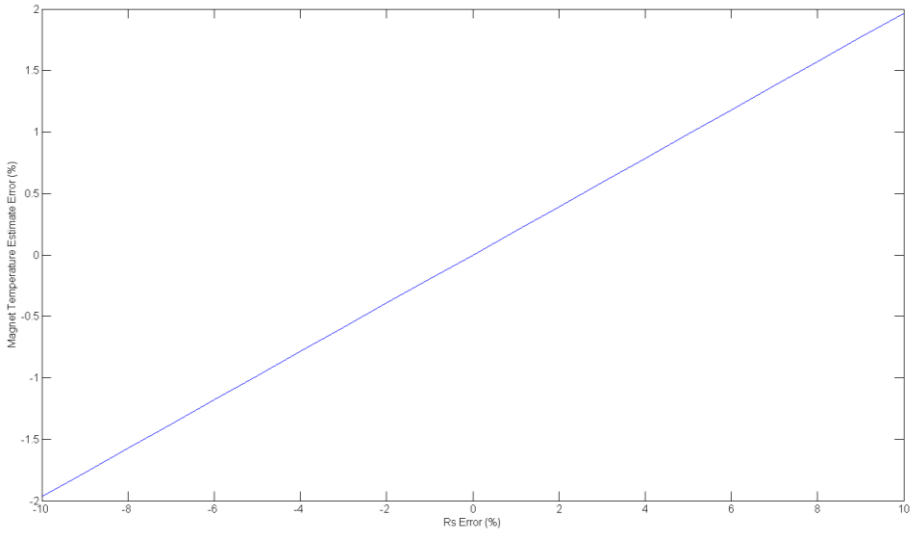

Figure 22: Stator resistance sensitivity test. Magnet temperature error Vs % error in Rs

The plot shows that with a 10% resistance error the magnet temperature estimate will vary by less than 2%. This highlights the difference in magnitude between the resistive and inductive terms at the operating speed of the machine, allowing this method to be relatively immune to stator resistance error.

4.2.3.4 Voltage Demand Inaccuracy Test

The voltage used in the observer is actually the q-axis voltage demand at the input to the PWM block. In an ideal drive system this is representative of the voltage at the motor winding. However, when considering the drive on which this technique is to be implemented there are several variable voltage drops between the internal signal and the voltage actually applied across the motor windings. These drops are caused by the non-linearity of the switching patterns and current shaping, the on-state IGBT resistances

and the resistive and inductive voltage drop across the long (up to 3m) phase connection harness.

The aim of this test is to ascertain what effect this variation will have on the temperature estimation. This is simulated by simply scaling the Vq value in the observer model. This does not replicate exactly the effects described but it will give an idea as to the sensitivity of the estimate to a variation in the Vq voltage from the demanded value.

Figure 23 shows the observer and actual magnet temperatures for a simulated heat-run. The different series on the plot are the actual magnet temperature as well as the estimated temperature when the voltage is scaled by + and – 3%.

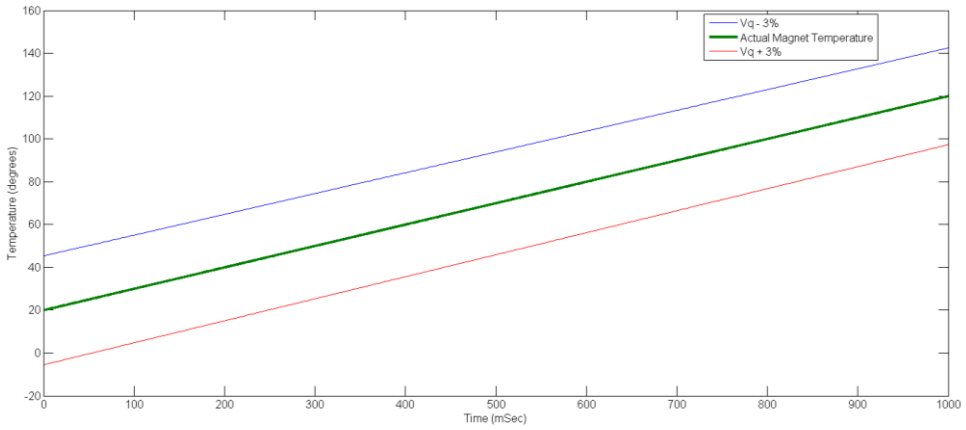

Figure 23: Voltage error sensitivity test.

The plot shows that a small error in the estimate of the Vq terminal voltage has a dramatic effect on the overall temperature sensing. A discrepancy between the demanded value and the actual value seen by the machine is

unavoidable; however this error can be compensated for within the experimental implementation.

4.2.3.5 Current Sensing Error Test

In the real system the current measurements for the inverter come from the LEM measurements and the analogue to digital converters. These measurements must be scaled and have the offset checked to ensure accurate representation of the machine current. It is very possible that there may be slight inaccuracies in this measurement and critically between different sets of power electronics.

This test is designed to show how susceptible to those inaccuracies the observer is. It is simulated in a very similar way to the voltage test; the current fed into the observer is scaled slightly from that which is going to the machine model. This error varies from -5% to +5% of the q-axis current and the results of this test can be seen in Figure 24.

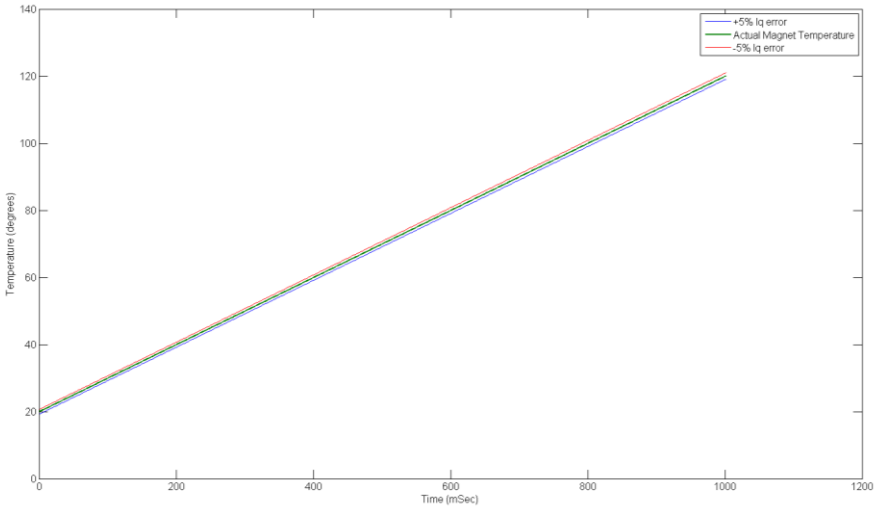

Figure 24: Current sensing error test.

It is clear from the plot in Figure 24 that the significance of these errors is very small compared to that of a voltage error. These errors do not require too much attention given the accuracy of available current sensing and the small effect these errors have on the final temperature estimation.

4.3 Conclusions

The above tests show that the proposed method seems robust to different load levels and speeds given accurate knowledge of the terminal voltage, rotor speed, stator currents and impedances. The sensitivity tests also show that the most critical parameter when considering the resulting error in temperature estimation is the stator terminal voltage. A 3% error in terminal voltage can give over a 20°C error in temperature estimation.

Unfortunately, this is a parameter which is difficult to measure and not measured in this application, so the information about the terminal voltage is to be obtained from the demanded values. It is well established that when using a PWM inverter the demanded voltage is in fact different to the voltage seen by the machine. In a standard vector controlled system this error is not a problem as the controller will simply increase the demand value until the stator current matches the demand.

The effects of the power electronics converter can be separated into two parts; firstly there are harmonic distortions caused by the switching and dead time effects and secondly there is a constant attenuation due to the voltage drop across switches and passive components. There are many published techniques to compensate for the non-linearity, many focussing on compensation of dead time and switching effects with the aim of improving the harmonic content of the waveforms applied to the machine

[49] [50] [51]. The dead time effects tend to average over an electrical cycle meaning that their effect may be to create noise on the temperature estimation but the mean value will not be affected; therefore given the relatively long thermal time constants these effects can be simply filtered or averaged out within the estimation procedure to avoid implementing complex control algorithms.

The effects of voltage drops across passive devices and cables cause a greater problem; they will cause a distortion with a DC error component between the demanded value and the actual voltage seen at the machine terminals. This error will be dependent upon the load current and could be estimated with accurate knowledge of the on-state resistances of the switching devices and the transmission line impedances. This could also be accounted for during a commissioning process where the effect of this error can be easily measured and then subtracted from the estimate within the observer.

5 Development of Stator Impedance Monitoring Scheme

This section is targeted at the traction machine introduced in Section 1.2.1 and whose specifications are given in Figure 4. A key failure mode for the machine design is an open circuit winding fault and this chapter analyses the performance of the machine under this fault condition. The fault of interest is first described, followed by analytical investigation to highlighting the effect of the fault in terms of the machine equivalent circuit and dynamic equations. The chapter then contains results obtained from finite element analysis of an example machine, confirming the effects of the fault.

5.1 Fault Definition

This section will first define the style of winding topology considered in this paper. It will then go on to define the fault in more detail, explaining the relevance of such faults to the machine design.

5.1.1 Machine Topology

The machine being analysed in this paper has multiple parallel concentrated delta windings supplied from one 3-phase inverter (Figure 25).

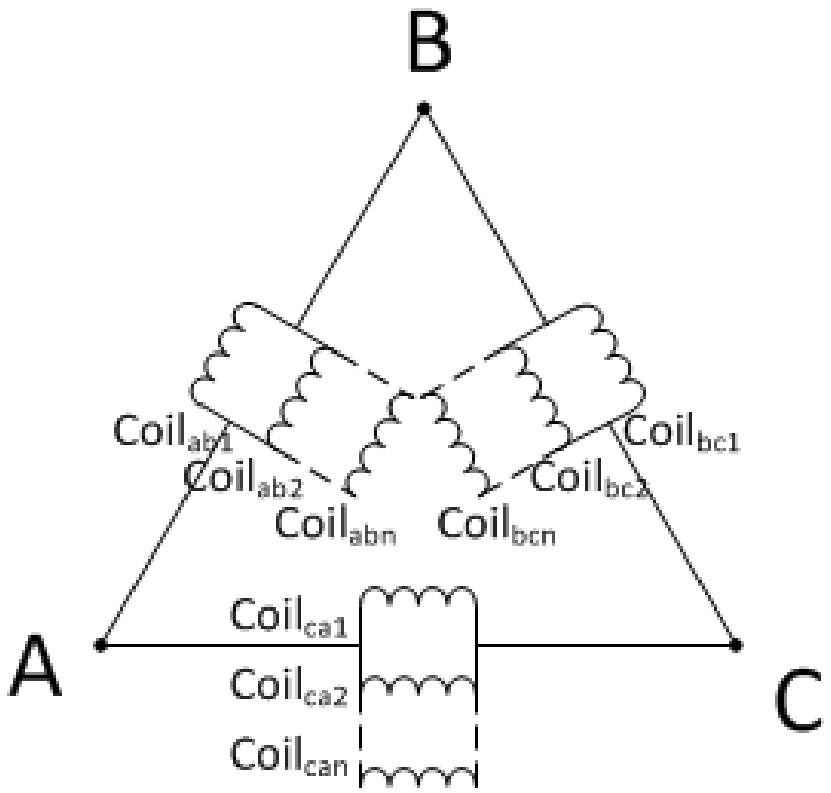

Figure 25: Delta winding with n parallel coils.

The rotor is constructed of standard IPM laminations, with axially segmented magnet skewed in 5 steps to give reduce torque ripple and back-emf harmonics.

5.1.2 Winding Fault

The parallel coils for each phase are connected internally and a single contact is exposed within the terminal box. When looking at this topology the weakest point is at the solder join of the coils to the terminal connector. Machines in aerospace and automotive applications often experience high temperature variations and severe vibrations which could put these joints

under stress and potentially lead to a coil becoming disjointed, creating an open-coil fault. The fault considered here is a total severing of one coil, meaning that the affected phase has n-1 coils connected and the final coil is then isolated from all other contacts.

This fault is of particular interest as it was observed following durability testing of this machine in the early development stages and so is a known failure mode.

The detection of this fault is challenging due to the parallel connection of the coils in each phase of the machine. This is because the back-emf will not be immediately affected by such faults. Under low load conditions the fault could easily go unnoticed as the effect on phase currents and terminal voltages will be minimal. This is in contrast to a series wound or multi-phase fault tolerant machine where any open circuit would cause the loss of a phase; here the challenge would lie in the continued operation of the machine under some form of adapted control [52] [53] [54].

5.2 Analysis of Faulted Machine

5.2.1 Healthy Machine

Equation (34) is the per phase voltage equation of a permanent magnet machine.

$$V_{ph} = i_{ph}R_{ph} + \frac{d\varphi_{sph}}{dt} \quad \textbf{(34)}$$

The flux φ_{sph} contains a contribution from the magnet flux passing the coilφ_m, and the flux produced by the current in the coils$i_{ph}L_{ph}$. R_{ph} and L_{ph} are the phase resistance and inductance respectively.

Under normal operation the phase impedances are the parallel sum of the individual coil resistance and inductance. Assuming all coil resistances (R_{coil}) and inductances (L_{coil}) are equal, the phase resistance and inductance can be defined as $\frac{R_{coil}}{n}$ and $\frac{L_{coil}}{n}$ where n is the number of parallel coils per phase. The per phase equivalent circuit can also be drawn as in Figure 26.

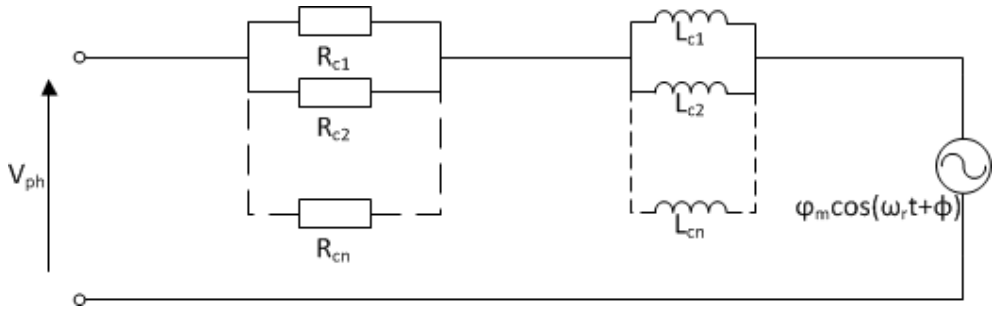

Figure 26: Per phase equivalent circuit of a parallel wound machine.

Equation (35) shows an equivalent two phase (αβ) representation of the machine equations.

$$V_{\alpha\beta} = i_{\alpha\beta}R_{ph} + \frac{d\underline{\varphi}_{sph}}{dt} \quad \textbf{(35)}$$

5.2.2 Faulty Machine

In the case of an open circuit fault, the affected phase will have one less coil connected in parallel. This means that the phase resistance and inductance for this faulty phase will be calculated by $\frac{R_{coil}}{n-1}$ and $\frac{L_{coil}}{n-1}$ respectively. It can be

seen that the impedances will increase because of this open circuit and that the effect will be more severe for a fewer number of parallel paths.

Equations (36)-(38) show the set of steady state per phase voltage equations for a machine with an open circuit coil on phase A.

$$V_a = i_a \frac{R_{coil}}{n-1} + \frac{d}{dt}\left[i_a \frac{L_{coil}}{n-1} + \varphi_m \cos(\omega_r t)\right] \quad \textbf{(36)}$$

$$V_b = i_b \frac{R_{coil}}{n} + \frac{d}{dt}\left[i_b \frac{L_{coil}}{n} + \varphi_m \cos\left(\omega_r t + \frac{2\pi}{3}\right)\right] \quad \textbf{(37)}$$

$$V_c = i_c \frac{R_{coil}}{n} + \frac{d}{dt}\left[i_c \frac{L_{coil}}{n} + \varphi_m \cos\left(\omega_r t - \frac{2\pi}{3}\right)\right] \quad \textbf{(38)}$$

This will cause a phase imbalance. Under the same speed and load condition as a healthy machine the terminal voltage must increase on the faulted phase to overcome the increased resistance.

Transforming these equations into their two phase equivalent will also show a similar effect. It will cause an unbalance by changing either the alpha or beta values with respect to a healthy machine depending on which phase contains the open coil. Equations (39) and (40) show the situation where a coil in phase A is opened.

$$V_\alpha = i_\alpha \frac{R_{coil}}{n-1} + \frac{d}{dt}\left[i_\alpha \frac{L_{coil}}{n-1} + \varphi_m \cos(\omega_r t)\right] \quad \textbf{(39)}$$

$$V_\beta = i_\beta \frac{R_{coil}}{n} + \frac{d}{dt}\left[i_\beta \frac{L_{coil}}{n} + \varphi_m \cos\left(\omega_r t + \frac{\pi}{2}\right)\right] \quad \textbf{(40)}$$

Given stable vector control the machine performance should be reasonably consistent; providing the required average torque and so able to maintain the demanded speed value.

However, there are issues which could go unnoticed; magnetic imbalances will cause a torque ripple and so extra vibrations at the rotor speed for a single coil fault. Another problem is the increased loading on the remaining coils; each must carry an extra $\frac{1}{n-1}\%$ of current to maintain the same load as the healthy coils.

If the machine is operated under full load then the coils of the faulted phase will be operating in an overload condition, this will cause increased copper losses and so additional heating. For machines not often operated near maximum load and with large numbers of parallel paths this could be acceptable for a long period of time, but the imbalanced magnetic circuit, added vibrations and extra losses will inevitably shorten the lifetime of the machine. However, this could rapidly become an issue in machines which are often heavily loaded where overheating and the potential for cascaded failures would become increasingly likely.

5.2.3 Finite Element Simulation

The faulted situation has been modelled in the Ansys Maxwell finite element simulation package. The fault itself has been created in the circuit editor by inserting a resistance between two of the coils in phase A. Assigning and large value to this resistance will simulate the occurrence of an open circuit fault.

Figure 27 shows the no load back-emf for both the healthy and faulted condition. As could be expected, under no load the fault has very little effect and its detection would be extremely difficult. In Figure 28 however, when the machine is loaded there is a clear imbalance on the faulted phase, which also shows in the two phase representation as the analysis implies.

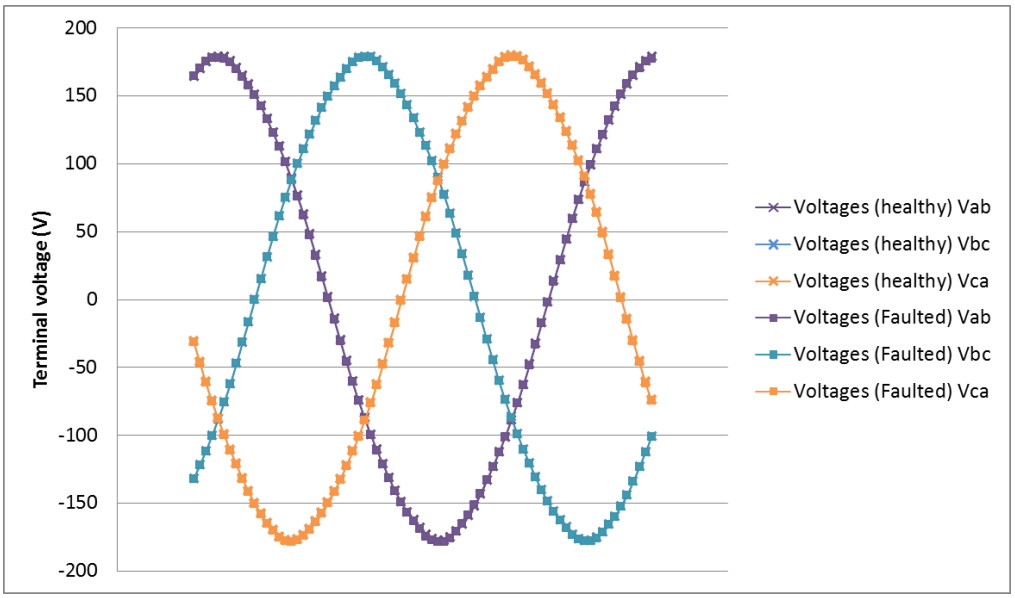

Figure 27: Terminal voltages for healthy and faulted machines under no load conditions

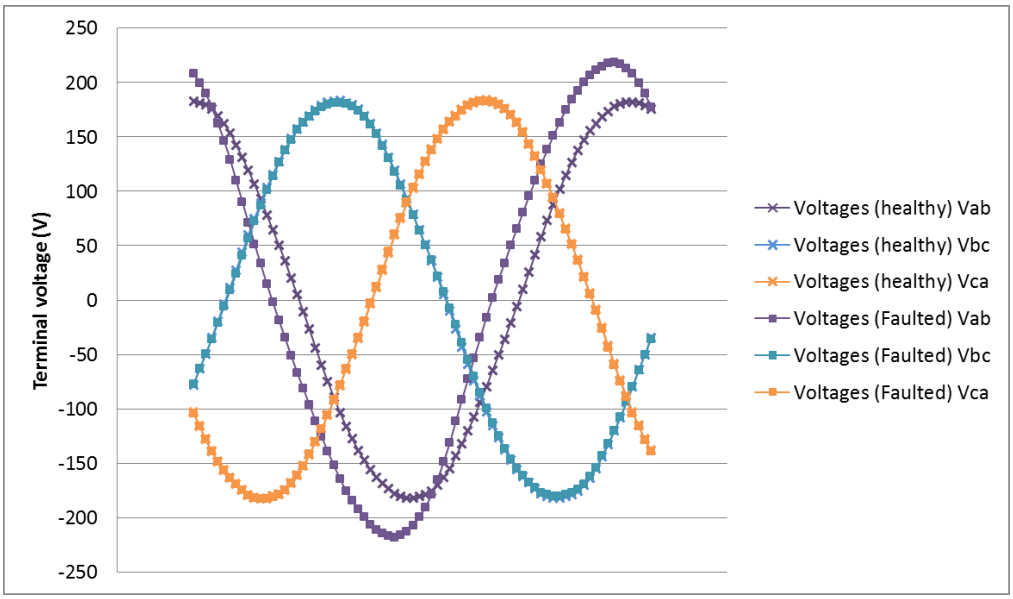

Figure 28: Terminal voltages for healthy and faulted machines under loaded conditions

As suggested above, a small variation in the torque ripple can be observed in Figure 30, caused by the uneven flux distribution around the air gap as can be seen in the flux plot of Figure 29.

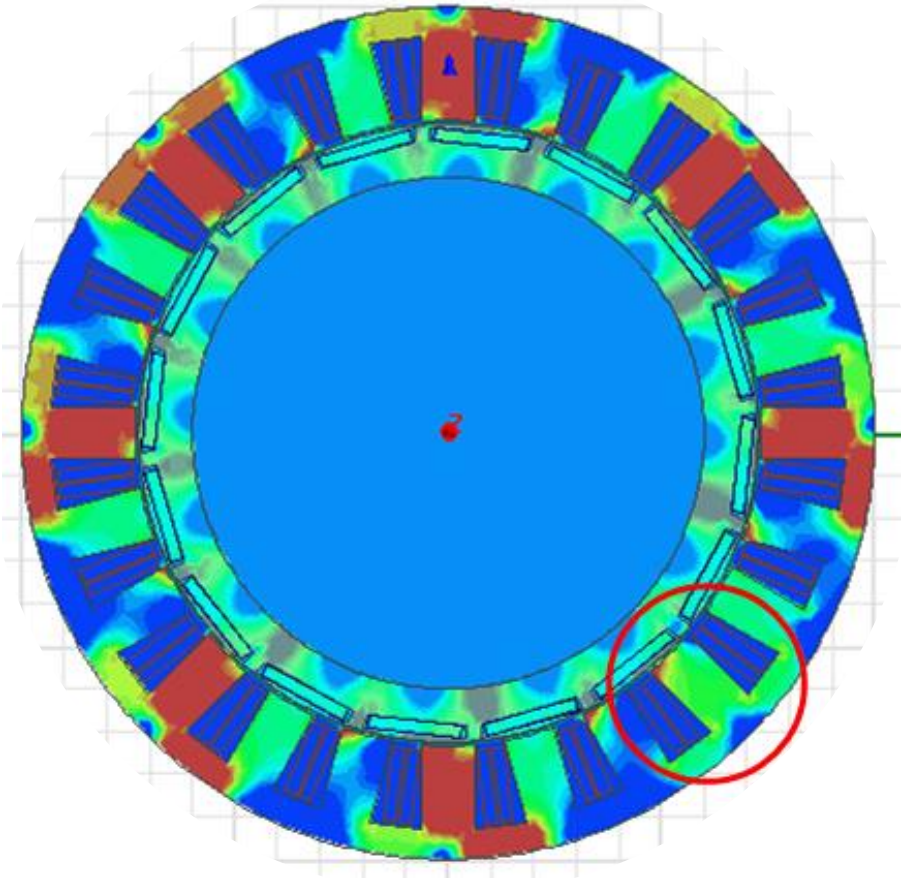

Figure 29: Magnetic field density plot of the faulted machine (open coil highlighted) under load conditions.

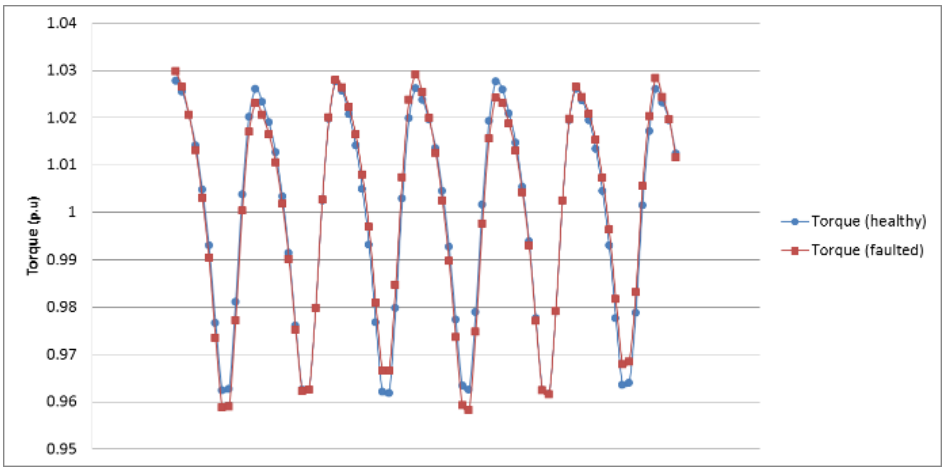

Figure 30: Developed torque (per unit) for a healthy and faulted machine under load conditions over one electrical cycle.

5.3 Conclusions

The load cycle for machines in a hybrid EV drive system is often very harsh. The machine is mainly operated under full or overload conditions with high torque transients. The analysis shows that an open circuit fault in this winding topology is more prominent under the high load conditions seen by a machine in this application.

The simulation of this scenario has confirmed the theoretical analysis. It shows that while an open circuit fault in a parallel wound machine does not necessarily cause dramatic performance degradation for the majority of the operating range; though the potential for thermal issues are increased at high and extreme loads. However continued operation in this state will inevitably force the machine to work harder to deliver equivalent performance and so shorten the lifetime and cause additional torque ripple which could potentially damage other components in the driveline.

6 Experimental Results

6.1 Experimental Rigs

The experimental element of this thesis was carried out across two sites, one facility being in the University of Nottingham and the second in the testing facilities at Cummins Generator Technologies' Stamford site. The following two sections of this chapter will briefly describe the set up at each location and chapter 8 will then present the results obtained.

6.1.1 University of Nottingham Test Facility

The test rig in Nottingham is comprised of a separately excited DC load machine mounted on a flexible test bed allowing coupling to a variety of test machines as can be seen in Figure 31. The machine is driven by a controlled DC drive which can be programmed to run through test routines in either torque or speed mode for various test scenarios.

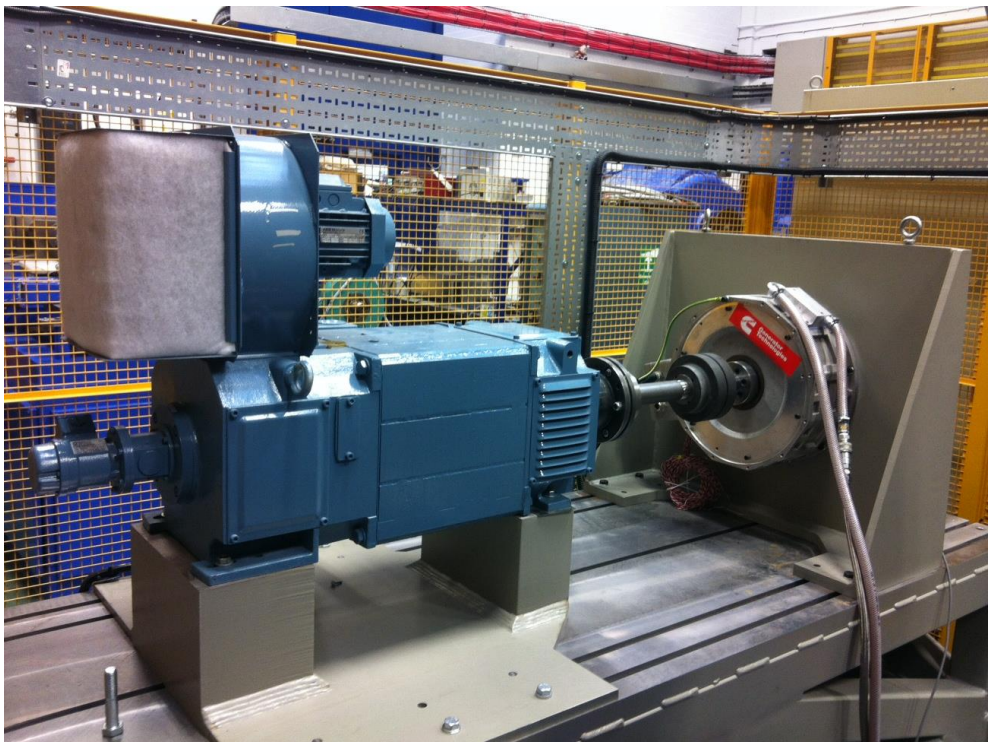

Figure 31: University of Nottingham test facility

The machine under test for the purpose of this thesis is the 8-pole, dual star wound interior permanent magnet machine, introduced in Section 1.2.1. This is driven using a Semikron SKAI 2 drive module and controlled using a DSP/FPGA solution developed within the University of Nottingham PEMC group.

The IPM on test is a water cooled machine and so a controlled water cooling system is used to enable testing to be performed under load. Finally and external encoder is located on the rear of the test bed (as shown in Figure 32) – the device chosen is a hollow shaft device meaning that it can be located between test machine and load machine if testing its use is required on a test machine with no access to the shaft from the rear.

Figure 32: Encoder mounted on rear of the test machine

6.1.2 Cummins Generator Technologies Test Facility

The test facility at the Cummins Generator Technologies site in Stamford is of a similar design; though customised more to suit the specific test machine (Figure 33). This again utilises a separately excited DC machine but driven by a 2 quadrant DC drive – allowing motoring or regeneration in a single direction.

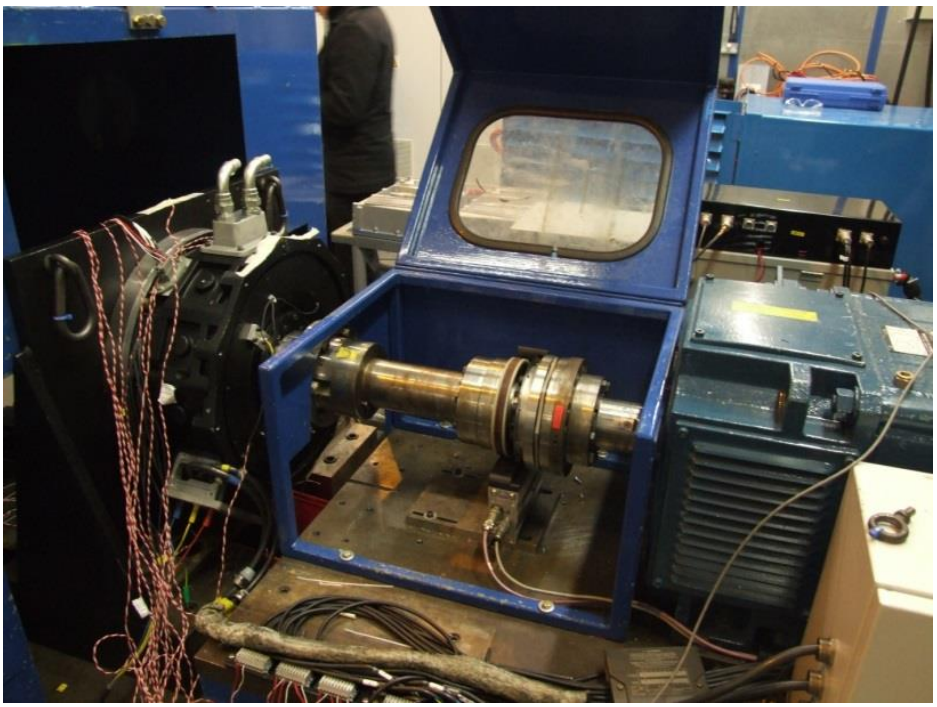

Figure 33: Test bed at Cummins Generator Technologies, Stamford

The machine under test in this location is the multiple parallel delta wound machine as described in Chapter 5. The current test cell set-up uses SKAI 2 modules to power the test machine; this is controlled using a SHARC DSP and Altera FPGA combination developed by Cummins Generator Technologies.

6.2 Implementation of Magnet Condition Monitoring

The decision was made to implement the observer on the Cummins test facility because of the availability of the control variables and base code to be passed into the observer and the relatively rapid prototyping functionality for the development of the estimation algorithms.

This means that the observer will be written in C-code alongside the current test cell control software. The temperature and speed constant will then be transmitted over the CANbus to the control computer.

This chapter will describe the tests required to linearise certain effects and to ensure the feasibility of the method for a defined machine and power electronics converter and then will go on to display some results obtained.

6.2.1 Non-linearity Caused by Iron Saturation

As the current loading within a PM machine increases, the level of flux travelling around the iron can cause saturation. This can limit the ability of the magnet flux to link with the stator coils, causing an effective lowering of the speed constant and this will appear as an artificial temperature rise when using this estimation method.

The proposed test to quantify and alleviate this effect is to monitor the constant relationship between the q-axis current and the developed torque over the required load range. If the iron is beginning to saturate at high loads then this will cause a flattening of the Iq vs. torque curve; meaning that at high loads a larger increase in Iq would be required for the same increase in torque production.

If this effect is not visible or negligible over the operating range then the effect can be ignored for this design. However if it is a clear effect then further investigation is required to characterise the effect of load on the back-emf in order to isolate and nullify the effect from the temperature observer.

The experimental results of the test can be seen in Figure 34. Despite a minor non-linearity being observable in the plot, the results give a

satisfactory level of confidence that an iron saturation related compensation scheme will not be required in the standard operating range of the machine.

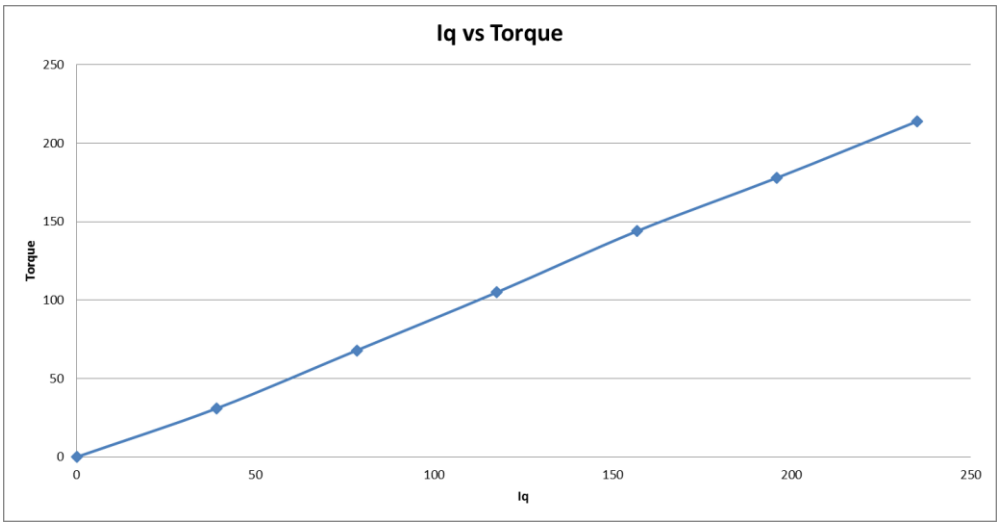

Figure 34: Iq vs. Torque. Id=0 control, constant rated speed.

6.2.2 Initial Estimation

An initial attempt at speed constant estimation was carried out. This test was to assess the accuracy of the observer with no additional linearization and with simple averaging over 500 calculations. It can be seen in Figure 35 that over the temperature range the observer produces an estimate of the speed constant with a linear inverse relationship to the measured rotor temperature. This shows that the observer has reliably isolated the change in temperature and this could be used to estimate the temperature variations given constant load operation of the machine. It does however highlight a variation with load; the next test is then designed to investigate and account for this variation.

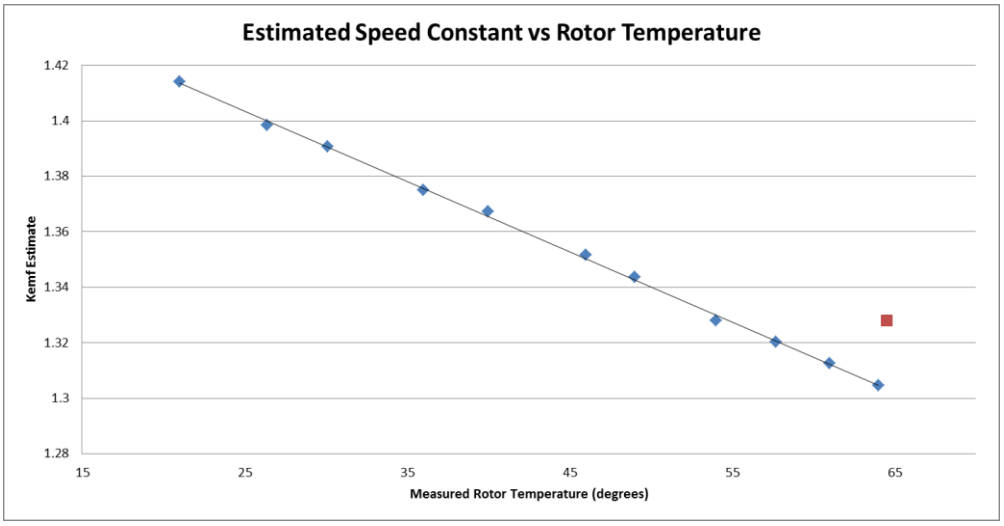

Figure 35: Estimated Speed Constant vs. Rotor Temperature. Trended Series - 30kW, Id = 0, rated speed. Square - 15kW, Id = 0, rated speed.

6.2.3 Variation with Load

A simple test where the machine is characterised across it load range will allow the estimate of the speed constant to be plotted against load level in Figure 36. A linear curve fit was found for this data which is shown in the plot and then this is accounted for in the observer.

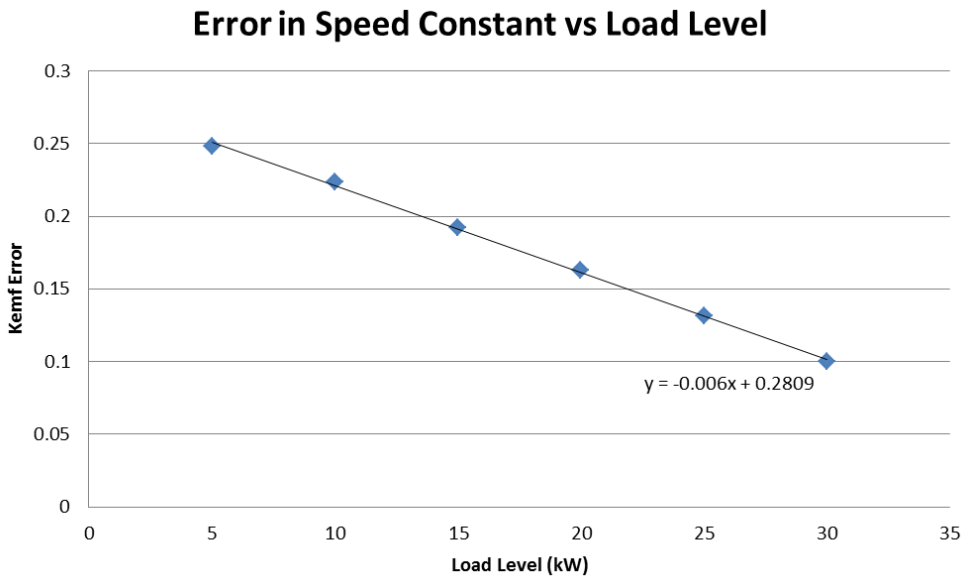

Figure 36: Error in Speed Constant vs. Load Level. Id = 0 control, constant rated speed.

The actual cause of these variations is a little more complex and originates mainly from a difference between the control V_q demand and the actual voltage seen at the machine terminals. The set up with two parallel SKAI modules brings with it a compulsory choke inductance to allow the outputs of the modules to be connected safely together, but unfortunately one of the disadvantages of this is a larger voltage drop across the transmission line between power electronics and machine. This voltage drop depends on the load current. Other contributors to the error are the effects of dead-time in the power converter and the voltage drops across the power devices themselves.

6.2.4 Commissioning Process

The method has been shown to be practical given the correct commissioning process and knowledge of the system parameters. There are several steps required to set up and calibrate the method for each machine in order to extract a reasonable temperature estimate for the operating range of the machine.

1. Map the machine Back-EMF vs. Temperature at rated speed. This will allow extraction of the speed constant at various temperatures which then gives a look-up table for the final step of the estimation.
2. Check Iq vs. Torque for the machine range, ensuring a linear relationship. If non-linear then this must be accounted for in the observer by either a look-up table or a curve fit to subtract the error.
3. Plot the error vs. load level, obtain a curve fit and allow for this within the observer.

Once these steps have been completed then the observer should be ready to provide an online temperature estimate.

6.2.5 Conclusions

This section introduces several rotor temperature monitoring techniques of varying complexities. These techniques range from physical measurements to signal injection. A model based observer method is chosen and thoroughly investigated in simulation to check the feasibility of the technique. The final section of the report then describes an experimental implementation of the observer, highlighting the challenges seen and introducing a commissioning process to overcome some of the challenges.

The implemented observer gives a clear linear relationship between rotor temperature and estimated speed constant given a constant load level. This means that the rotor temperature can easily be tracked under steady state conditions using this method. The difficulty arises when load levels or system parameters change due to the model based nature of the method. A commissioning process has been defined to eliminate these issues, the effectiveness of which will only be proven in practice by gathering test results from different situations. Further testing will be required to identify the specific accuracy of the method and as mentioned above, the robustness and effectiveness of the commissioning process.

A demagnetised rotor in any closed loop system is quite benign to any end user and so the safety implications of this fault are not immediately obvious. It requires a deeper examination to explain why the detection of magnet demagnetisation or rotor over temperature are useful in terms of functional safety. It is clear that one effect of reduced magnet flux is an increased current demand to achieve an equivalent torque; this increased current demand, while still being within the capability of the system may cause greater stresses on certain components than assumed during the design process. This will shorten the life of these components and eventually could cause them to fail prematurely; this second failure could certainly be one which directly affects the safety of the driver.

In this scenario the first fault (demagnetisation) is known as a ‘latent fault’ which left unaddressed could cause a second more serious fault, bridge short circuit due to device overstress for example. Therefore the detection, prevention or mitigation of the latent fault will reduce the occurrence of thee second, more safety critical fault.

6.3 Initial Position Detection Scheme

Any sensorless control scheme has a period of uncertainty while the rotor position is located initially. This is where all of the integrator states settle to their steady state values and the phase locked loop or observer locks onto the rotor position. This can be a very short period of time (a few ms) but it could result in large currents and potentially damaging magnetic fields in the machine for this initialisation period; therefore an initial position detection scheme is necessary.

The scheme proposed by Kim et al [55] is to be completed at zero speed before the current and power controllers are initialised. It is carried out in two phases, firstly the HF inject scheme described in section 2.3.1.3 is applied for a short period until the estimation settles and locks onto the d-axis. This process can be very short, in the order of milliseconds an example of the output from this technique implemented on the Nottingham test rig can be seen in Figure 37. At this stage it is still unclear whether the estimate is of the north or south pole of the machine and so to enable the controller to function correctly further steps must be taken to derive this information.

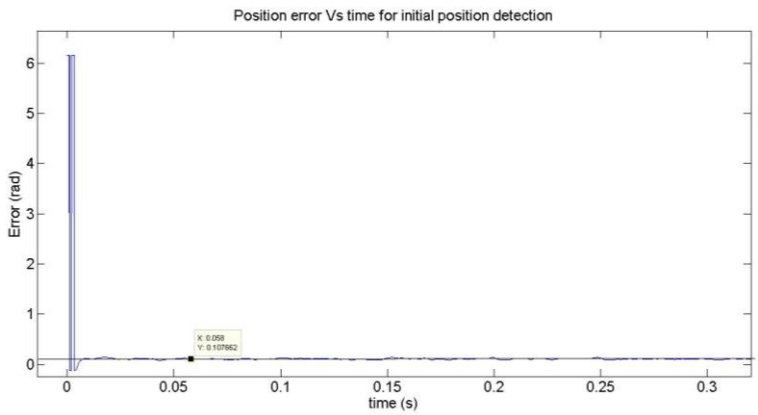

Figure 37: Settling time for HF-injection at start-up

6.3.1 Pole Detection

The next stage of the initial position identification scheme is to find out which pole the algorithm has locked onto, and to correct if necessary. The technique adopted is described in [55] which is based on the relationship between iron saturation and inductance. A voltage is applied along the estimated d-axis, this will set up a flux which will either assist or fight against the flux produced by the magnets (Figure 38).

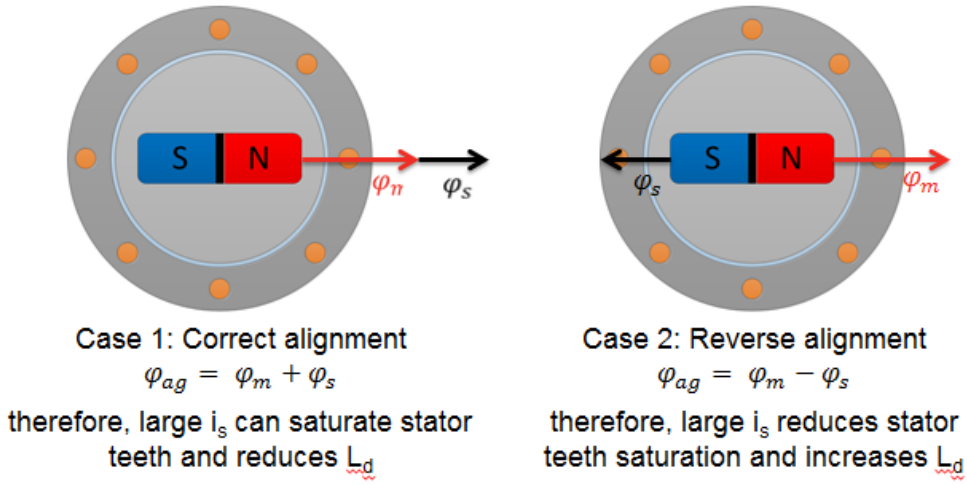

Figure 38: Effect of d-axis voltage pulses

The case where the voltage is in the correct polarity, so that the flux aligns with the magnet flux and the rotor position is on the correct pole, then the stator iron will be forced to saturate to a higher level and so the inductance will decrease. The opposite case, where the polarity is incorrect, will cause an increase in the inductance.

This change can be detected by observing the transient current response to the applied voltage. The transient current response to this step change is

defined in equation (41). This shows that as L_d increases then the current will rise more slowly for a given voltage, therefore if the voltage pulse is applied for a short, fixed time then a higher current peak will be seen for a lower inductance.

$$i_d = \int \frac{V_d}{L_d} dt \quad \textbf{(41)}$$

By monitoring the current response to the two voltage pulses it is clear which occasion sees the higher inductance and so which pole has been detected.

The complete algorithm follows the steps below:

1. Apply a voltage pulse at estimated rotor position = 0 for a fixed short period. The pulse should be high enough to create a measurable spike that is still increasing linearly at the end of the pulse
2. Allow current to dissipate back to 0
3. Apply a symmetrical voltage pulse at estimated rotor position = 180
4. Compare the two peaks of the current response as in Figure 39. If the first is higher the angle is correct, if not then add 180° to the estimated electrical angle.

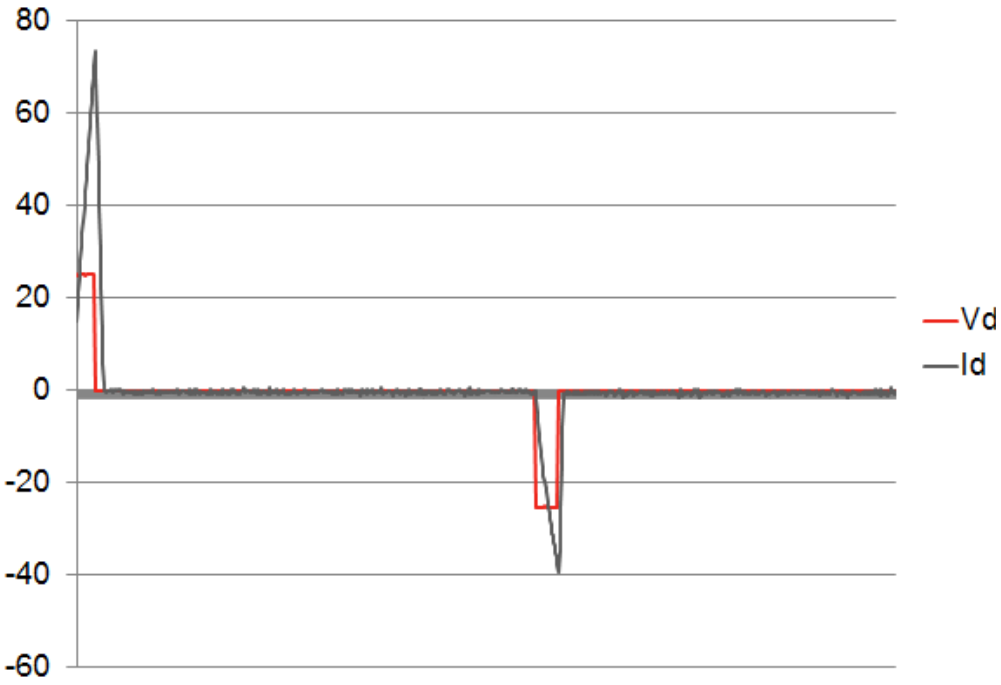

Figure 39: Experimental measurement of current response along positive and negative d-axis

6.3.2 Conclusion

The result of the steps described above is an initial rotor angle estimate which can be used to initiate vector control. The potential uses for this technique in automotive are promising as an initial check of the rotor position sensors functionality – the short duration of the injection pulse required could be an acceptable disturbance at vehicle ignition. There still remains challenged to utilising such a scheme to remove the rotor position sensor altogether in many applications given the need for current injection for the duration of time that the machine is at very low speeds and the EMC issues this brings.

7 Conclusions

The aims of this thesis were threefold; first to gain an understanding of the push for higher levels of fault diagnostics and condition monitoring within the automotive industry, secondly to review and develop techniques to monitor the condition of the rotor magnets in real time on a PMSM based automotive electrical drive system and finally to review the applicability and use of sensorless control as a way to mitigate faults relating to current sensing.

This thesis has achieved the first aim by providing a comprehensive review of a current, prominent standard which must be considered when designing a new product for the automotive industry, especially one targeted at a safety critical application such as powertrain or steering related electronics. ISO26262 [5] is one of a number of standards and controls in place to ensure that any product present on the roads will respond in a safe manner under all reasonably expected conditions, including subcomponent failures. The level of analysis and verification required has been described in detail in chapter 2, looking into each part of the standard and relating it directly to the relevant product design stage. It is clear that the drive for safety is pushing manufacturers to develop more robust components and thus reduce the occurrence of faults analysed within product FMEAs as one solution to aid compliance. Where components cannot be made reliable enough to not require additional mitigation then the standard is also driving engineers to develop ways of detecting these faults and innovative methods of mitigating the unsafe reactions. This detail has created new areas of research pushing

the boundaries of fault detection and tolerance as well as work into the physics of failure to increase subcomponent reliability.

This provides the motivation for later chapters which go on to describe and implement techniques which can be utilised for fault detection, mitigation and tolerance. The second aim is then addressed; a method to detect or predict faults relating to the magnets within a permanent magnet motor is derived and implemented. This is achieved by use of a real-time model which extracts a variable proportional to the magnet temperature. The variable can be monitored to provide temperature estimations to limit overuse of the system, reducing the likelihood of faults occurring and ensuring that operation remains within safe limits. Trends of this variable can also be used to monitor magnet condition; discontinuous behaviour of the variable would likely indicate a step change in magnet flux which would be an indicator of physical damage. In the scope of automotive safety this could then drive a safe shutdown of the system before any uncontrollable and unsafe behaviour manifests. The third objective is then tackled as this thesis shows how safe operation of a motor drive system is possible following a fault rendering the rotor position sensor inoperable or inaccurate. There are various control methods offered to cover a range of operating conditions which can then be employed in the relevant scenarios as called out by a failure mode analysis or other safety work product. The shortcomings are also highlighted, namely being the challenge to maintain silent operation and to meet electromagnetic compatibility requirements set by vehicle manufacturers. These shortcomings have led to the conclusion that currently sensorless control techniques can only be applied in limited circumstances; where only high speed operation is required or at time where

short term deviations from noise specifications are acceptable. Further work is still required in this area, work to enable the detection of rotor position with less disturbance to the fundamental current waveform; either by innovative machine design or by new modulation techniques. The model developed in chapter 3 has the potential to aid this research.

The progression towards greater autonomy on the roads; vehicles being able to navigate, communicate and control themselves to a predetermined destination is forcing ever increasing safety demands onto the automotive industry. Random failures mean that fault detection, back-up controls and ever increasing redundancy are becoming common place in the design of new automotive technologies. Redundancy however comes at a cost; volume, weight and price are all critical characteristics in an automotive system, all of which are inevitably increased if redundancy is implemented to tackle subcomponent reliability issues. The trend within the industry is clearly for vehicle to get lighter, safer and more cost effective with greater reliability and availability. This means that the obvious solution of redundancy does not fit. Innovative back-up control methods and preventative fault detection methods which alleviate the need for multiple redundant components within a system offer a cost effective solutions; this is a good reason why the demand for research into fault mitigation is growing and will continue.

8 Further Work

This area of research offers a vast amount of scope for further work. With the push for autonomous driving and the ever increasing safety and reliability demands this brings the industry must focus on innovative ways to reduce the occurrence of safety critical faults.

This thesis specifically offers scope to develop further the rotor magnet condition monitoring technique; numerous algorithms could be developed to detect patterns in the variation of the rotor flux constant in various conditions. The author can envisage further projects which will progress the technique to observe and develop a far greater understanding of the impact of temperature on permanent magnet machine operation. The work could highlight further the trade-off between the cost of advanced cooling techniques and performance given the direct link demonstrated in this thesis between a rotor magnet temperature and torque constant. Potential projects could be;

1) Further development and upgrade of the method and algorithms to monitor the magnet condition by tracing the rotor flux along the B-H curve of the magnetic material.
2) Investigation of the technique's ability to detect partial or full demagnetisation of rotor magnets using FEA and the impact this has on the estimation of temperature.
3) Investigation into advanced control techniques and the potential to compensate for the magnet flux reduction by adjusting the angle of

the applied voltage vector; effectively applying a positive I_d to boost rotor flux.

Opportunities also exist to develop schemes to exploit the stator fault detection methods discussed. A mature and validated variant of this technique could be used on a commissioned system to monitor for any fault leading to a change in stator impedance, for example a resistive phase connection caused by corroded terminals would exhibit a not too dissimilar effect. It may also be interesting to assess the applicability of the proposed technique to turn to turn short circuits within individual windings, where the short effectively reduces the impedance of the winding as a whole.

The simulation developed in chapter 3 offers opportunities to investigate the potential uses of fundamental wave PWM modulation. The potential investigations could look in detail at current waveform distortions caused by the edge shifting algorithms and look to optimise these with an aim of reducing the noise created by the modulation techniques. A further opportunity lies in the co-simulation with a finite element package, work by Arellano-Padilla et al [56] investigates the information which can be extracted from the machine using fundamental wave excitation. The initial simulation of the technique was developed using a co-simulation based around this model [57].

The final area where further work could be carried out with functional safety in mind would be to assess the robustness of these detection and tolerance techniques. This would then be used to justify their implementation into a specific road vehicle system. This would involve performing fault insertion testing to demonstrate the effectiveness and robustness of the methods at

a vehicle level, demonstrating their effectiveness and the benefit they offer to driver safety over other current systems.

9 References

[1] G. Maggetto and J. Van Mierlo, "Electric and electric hybrid vehicle technology: a survey," in *Electric, Hybrid and Fuel Cell Vehicles (Ref. No. 2000/050), IEE Seminar* , 2000.

[2] R. Joshi and A. Deshmukh, "Hybrid Electric Vehicles: The Next Generation Automobile Revolution," in *Electric and Hybrid Vehicles, 2006. ICEHV '06. IEEE Conference on* , 2006.

[3] O. Momoh and M. Omoigui, "An overview of hybrid electric vehicle technology," in *Vehicle Power and Propulsion Conference, 2009. VPPC '09. IEEE* , 2009.

[4] Y. Du, S. Lukic, B. Jacobson and A. Huang, "Review of high power isolated bi-directional DC-DC converters for PHEV/EV DC charging infrastructure," in *2011 IEEE Energy Conversion Congress and Exposition*,, Phoenix, AZ, 2011.

[5] I. S. O. (ISO), *ISO26262 Road Vehicles - Functional Safety,* Geneva, Switzerland: ISO, 2011.

[6] D. Fodorean, M. Ruba, D.-C. Popa and A. Miraoui, "Fault tolerant permanent magnet machines used in automobile applications," in *Electrical Machines (ICEM), 2010 XIX International Conference on* , 2010.

[7] B. Mecrow, A. Jack, J. Haylock and J. Coles, "Fault-tolerant permanent magnet machine drives," *Electric Power Applications, IEE Proceedings ,* vol. 143, no. 6, pp. 437-442, 1996.

[8] L. Parsa and H. Toliyat, "Fault-Tolerant Interior-Permanent-Magnet Machines for Hybrid Electric Vehicle Applications," *Vehicular Technology, IEEE Transactions on ,* vol. 56, no. 4, pp. 1546-1552, 2007.

[9] M. Rahman, M. Masrur and M. Uddin, "Impacts of interior permanent magnet machine technology for electric vehicles," in *Electric Vehicle Conference (IEVC), 2012 IEEE International* , 2012.

[10] K. Wejrzanowski and J. Al-Tayie, *Considerations when developing a motor generator solution for green commercial vehicles,* 2012.

[11] S. Guttowski, S. Weber, E. Hoene, W. John and H. Reichl, "EMC issues in cars with electric drives,," in *Electromagnetic Compatibility, 2003 IEEE International Symposium on*, 2003.

[12] V. Rodriguez, "Automotive component EMC testing: CISPR 25, ISO 11452–2 and equivalent standards," *Electromagnetic Compatibility Magazine, IEEE,* vol. 1, no. 1, pp. 83-90, 2012.

[13] Department for Transport (UK), "Gov.uk," 05 Feb 2015. [Online]. Available: https://www.gov.uk/government/uploads/system/uploads/attachment_data/file/401295/quarterly-estimates-jul-to-sep-2014.pdf. [Accessed 08 Feb 2015].

[14] C. Edwards, "Safety engineering sets new challenges for electronic system design," *Engineering & Technology,* vol. 11, no. 7, pp. 72-74, 12 July 2016.

[15] T. Sebastian, "Temperature effects on torque production and efficiency of PM motors using NdFeB magnets," *Industry Applications, IEEE Transactions on,* vol. 31, pp. 353-357, Mar/Apr 1995.

[16] Arnold Magnetics, "Arnold Magnetics N42SH datasheet," 07 12 2015. [Online]. Available: http://www.arnoldmagnetics.com/Portals/0/Files/Catalogs%20and%20Lit/Neo/151021/N42H%20-%20151021.pdf?ver=2015-12-07-103816-973. [Accessed 7 11 2016].

[17] C. Mastorocostas, I. Kioskeridis and N. Margaris, "Thermal and slip effects on rotor time constant in vector controlled induction motor drives," *Power Electronics, IEEE Transactions on,* vol. 21, pp. 495-504, March 2006.

[18] J. Bates and A. Tustin, "Temperature rises in electrical machines as related to the properties of thermal networks," *Proceedings of the IEE - Part A: Power Engineering,* vol. 103, no. 11, pp. 471-482, October 1956.

[19] H. W. Kudlacik and D. M. Willyoung, "Local Rotor Winding Temperature Measurements for Large Turbine-Generator Fields," *Power Apparatus and Systems, Part III. Transactions of the American Institute of Electrical Engineers ,* vol. 81, no. 3, pp. 687-693, April 1962.

[20] M. Kovačić, M. Vražić and I. Gašparac, "Bluetooth wireless communication and 1-wire digital temperature sensors in synchronous machine rotor temperature measurement," in *Power Electronics and Motion Control Conference (EPE/PEMC), 2010 14th International*, 2010.

[21] I. Dolezal, "Simple telemetry system for a rotor temperature measurement," in *Applied Electronics (AE), 2011 International Conference on*, 2011.

[22] G. Jianzhong, G. Hui and H. Zhe, "Rotor temperature monitoring technology of direct-drive permanent magnet wind turbine," in *Electrical Machines and Systems, 2009. ICEMS 2009. International Conference on*, 2009.

[23] D. Varduca, C. Olivotto and H. Selegean, "Monitoring system for over-temperature detection of water cooled rotor poles of hydro electrical generators installed at the Danube River Iron Gates Power Plant," in *Energy Conversion Engineering Conference, 1996. IECEC 96., Proceedings of the 31st Intersociety* , 1996.

[24] E. de M Fernandes, A. Oliveira, C. Jacobina and A. Lima, "Comparison of HF signal injection methods for sensorless control of PM synchronous motors," in *Applied Power Electronics Conference and Exposition (APEC), 2010 Twenty-Fifth Annual IEEE* , 2010.

[25] M. Schroedl, "Sensorless control of AC machines at low speed and standstill based on the "INFORM" method," in *Industry Applications Conference, 1996. Thirty-First IAS Annual Meeting, IAS '96., Conference Record of the 1996 IEEE* , 1996.

[26] L. Wang and R. Lorenz, "Rotor position estimation for permanent magnet synchronous motor using saliency-tracking self-sensing method," in *Industry Applications Conference, 2000. Conference Record of the 2000 IEEE* , 2000.

[27] D. Reigosa, P. Garcia, F. Briz, D. Raca and R. Lorenz, "Modeling and Adaptive Decoupling of Transient Resistance and Temperature Effects in Carrier-Based Sensorless Control of PM Synchronous Machines," in *Industry Applications Society Annual Meeting, 2008. IAS '08. IEEE*, 2008.

[28] D. Reigosa, F. Briz, P. García, J. Guerrero and M. Degner, "Magnet Temperature Estimation in Surface PM Machines Using High-Frequency Signal Injection," *Industry Applications, IEEE Transactions on ,* vol. 46, no. 4, pp. 1468-1475, 2010.

[29] M. Ganchev, C. Kral, H. Oberguggenberger and T. Wolbank, "Sensorless rotor temperature estimation of permanent magnet synchronous motor," in *IECON 2011 - 37th Annual Conference on IEEE Industrial Electronics Society* , 2011.

[30] C. Kral, A. Haumer and S. B. Lee, "Innovative thermal model for the estimation of permanent magnet and stator winding temperatures," in *Energy Conversion Congress and Exposition (ECCE), 2012 IEEE* , 2012.

[31] A. Sarikhani and O. Mohammed, "Demagnetization Control for Reliable Flux Weakening Control in PM Synchronous Machine," *Energy Conversion, IEEE Transactions on ,* vol. 27, no. 4, pp. 1046-1055, 2012.

[32] A. El-Refaie, N. Harris, T. Jahns and K. Rahman, "Thermal analysis of multibarrier interior PM synchronous Machine using lumped parameter model," *Energy Conversion, IEEE Transactions on ,* vol. 19, no. 2, pp. 303- 309, 2004.

[33] X. Xiao, C. Chen and M. Zhang, "Dynamic Permanent Magnet Flux Estimation of Permanent Magnet Synchronous Machines," *Applied Superconductivity, IEEE Transactions on,* vol. 20, no. 3, pp. 1085-1088, 2010.

[34] E. d. M. Fernandes, A. C. Oliveira, A. M. N. Lima, C. B. Jacobina, W. R. N. Santos and R. D. Lorenz, "A metric for evaluation of the performance of saliency-tracking self-sensing control of PM motor," in *Brazilian Power Electronics Conference*, Gramado, 2013.

[35] S. C. Yang, Y. L. Hsu and G. R. Chen, "Design issues for permanent magnet machine sensorless drive combining saliency-based and back-EMF-based control in the entire speed range," in *IEEE International Conference on Industrial Technology (ICIT)*, Taipei, 2016.

[36] Y. Hua, Sensorless Control of Surface Mounted Permanent Magnet Machines Using Fundamental PWM Excitation (PhD Thesis), University of Nottingham, 2009.

[37] H. Jiang and M. Sumner, "Sensorless torque control of a PM motor using modified HF injection method for audible noise reduction," in *Power Electronics and Applications (EPE 2011), Proceedings of the 2011-14th European Conference on*, 2011.

[38] Y. Tauchi and H. Kubota, "Audible noise reduction method in IPMSM position sensorless control based on high-frequency current injection," in *Power Electronics Conference (IPEC-Hiroshima 2014 - ECCE-ASIA), 2014 International*, 2014.

[39] Y. Hua, M. Sumner, G. Asher and Q. Gao, "Sensorless control for a PM machine with reduced current distortion using space vector PWM excitation," in *EPE '09. 13th European Conference on Power Electronics and Applications, 2009.*, 2009.

[40] H. J, "Sensorless Position Control of Induction Motors - an Emerging Technology," in *Proceedings of AMC, Coimbra(Portugal)*, 1998.

[41] J. Cilia, G. M. Asher, K. J. Bradley and M. Sumner, "Control of a Shaft Sensorless Position Induction Motor Using an Asymmetric Outer Section Cage," *Proceedings of EPE (Trondheim),* vol. 4, pp. 486-491, 1997.

[42] M. Samimi, A. Mahari, M. Farahnakian and H. Mohseni, "The Rogowski Coil Principles and Applications: A Review," *Sensors Journal, IEEE,* vol. 15, no. 2, pp. 651-658, 2015.

[43] E. Robeischl and M. Schroedl, "Optimized INFORM measurement sequence for sensorless PM synchronous motor drives with respect to minimum current distortion," *Industry Applications, IEEE Transactions on,* vol. 40, pp. 591 - 598, 2004.

[44] T. Wolbank and J. Machl, "A modified PWM scheme in order to obtain spatial information of AC machines without mechanical sensor," in *Applied Power Electronics Conference and Exposition, 2002. APEC 2002. Seventeenth Annual IEEE*, 2002.

[45] J. Bottomley, C. Gerada and M. Sumner, "Electrical machine design for optimal self-sensing properties of SPMSMs," in *Power Electronics, Machines and Drives (PEMD 2012), 6th IET International Conference on* , 2012.

[46] A. Budden, R. Wrobel, D. Holliday, P. Mellor, A. Dinu, P. Sangha and M. Holme, "Impact of Rotor Design on Sensorless Position Estimation," in *IEEE Industrial Electronics, IECON 2006 - 32nd Annual Conference on*, 2006.

[47] SC. Yang, T. Suzuki, R. Lorenz and T. Jahns, "Surface permanent magnet synchronous machine design for saliency-tracking self-sensing position estimation at zero and low speeds," in *Energy Conversion Congress and Exposition (ECCE), 2010 IEEE*, 2010.

[48] D. Reigosa, K. Akatsu, N. Limsuwan, Y. Shibukawa and R. Lorenz, "Self-Sensing Comparison of Fractional Slot Pitch Winding Versus Distributed Winding for FW- and FI IPMSMs Based on Carrier Signal Injection at Very Low Speed," *Industry Applications, IEEE Transactions on,* vol. 46, no. 6, pp. 2467-2474, 2010.

[49] M. Seilmeier, C. Wolz and B. Piepenbreier, "Modelling and model based compensation of non-ideal characteristics of two-level voltage source inverters for drive control application,," in *Electric Drives Production Conference (EDPC), 2011 1st International* , 2011.

[50] N. Urasaki, T. Senjyu, K. Uezato and T. Funabashi, "Adaptive Dead-Time Compensation Strategy for Permanent Magnet Synchronous Motor Drive," *Energy Conversion, IEEE Transactions on ,* vol. 22, no. 2, pp. 271-280, 2007.

[51] G. Wang, D. Xu and Y. Yu, "A novel strategy of dead-time compensation for PWM voltage-source inverter," in *Applied Power Electronics Conference and Exposition, 2008. APEC 2008. Twenty-Third Annual IEEE*, 2008.

[52] D. Casadei, M. Mengoni, G. Serra, A. Tani and L. Zarri, "Optimal fault-tolerant control strategy for multi-phase motor drives under an open circuit phase fault condition," in *Optimal fault-tolerant control strategy for multi-phase motor drives under an open circuit phase fault condition," Electrical Machines, 2008. ICEM 2008. 18th International Conference on*, 2008.

[53] S. Dwari and L. Parsa, "Open-circuit fault tolerant control of five-phase permanent magnet motors with third-harmonic back-EMF," in *Industrial Electronics, 2008. IECON 2008. 34th Annual Conference of IEEE* , 2008.

[54] O. Jasim, C. Gerada, M. Sumner and J. Arellano-Padilla, "Operation of an induction motor with an open circuit fault by controlling the zero sequence voltage," in *Electric Machines and Drives Conference, 2009. IEMDC '09. IEEE International* , 209.

[55] H. Kim, K.-K. Huh, R. Lorenz and T. Jahns, "A novel method for initial rotor position estimation for IPM synchronous machine drives,," *Industry Applications, IEEE Transactions on ,,* Vols. vol.40, , no. no.5,, pp. 1369-1378, 2004.

[56] J. Arellano-Padilla, M. Sumner and C. Gerada, "Condition monitoring approach for permanent magnet synchronous motor drives based on

the INFORM method," *IET Electric Power Applications,* vol. 10, no. 1, pp. 54-62, 2016.

[57] J Arellano-Padilla, M Sumner, C. Gerada and G. Buckley, "Detection of inter-coil short circuits in the stator winding of a PM machine by using saliency tracking schemes," in *IEEE Energy Conversion Congress and Exposition*, Phoenix, AZ, 2011.

[58] R. I. Jones, "The More Electric Aircraft: the past and the future?," in *Electrical Machines and Systems for the More Electric Aircraft (Ref. No. 1999/180), IEE Colloquium on* , 1999.

[59] W. Pearson, "The more electric/all electric aircraft-a military fast jet perspective," in *All Electric Aircraft (Digest No. 1998/260), IEE Colloquium on* , 1998.

[60] R. Quigley, "More Electric Aircraft," in *Applied Power Electronics Conference and Exposition, 1993. APEC '93. Conference Proceedings 1993., Eighth Annual*, 1993.

[61] Y. Duan and H. Toliyat, "A review of condition monitoring and fault diagnosis for permanent magnet machines," in *Power and Energy Society General Meeting, 2012 IEEE*, 2012.

Appendix A: Review of ISO26262

1. Part 2: Management of functional safety

The second part of ISO26262 discusses the management of functional safety, defining a design methodology to assist in the creation of 'functionally safe' engineering solutions. While the standard does not claim to contribute to the nominal design and operation of the product, it does rely on a well-structured design process which it can align its safety design methodology to. Specifically this takes the form of the 'Safety Life Cycle' (Figure 40). Within the life cycle are contained several steps which must be taken throughout the design of a product to ensure compliance. The numbering of the items within the cycle points to the applicable part and chapter of the standard.

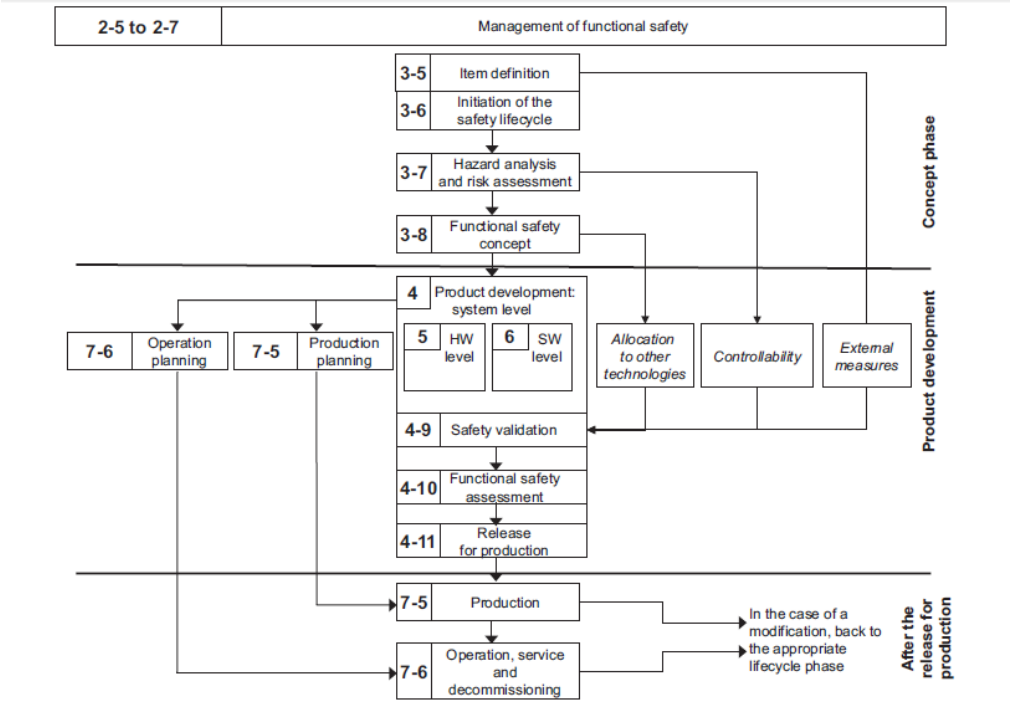

NOTE Within the figure, the specific clauses of each part of ISO 26262 are indicated in the following manner: "m-n", where "m" represents the number of the part and "n" indicates the number of the clause, e.g. "3-6" represents Clause 6 of ISO 26262-3.

Figure 40: Safety Life Cycle [4]

The top of the cycle relates to a concept design phase. This phase of a product design is generally where requirements are gathered and analysed to set the goals for the design itself. The concept phase also includes the initial architecture design; a top level block design describing the overall concept. It is this block level design that then enables the requirements to be broken down further into sub-system requirements to enable the detailed design of each block to be completed almost in isolation from the neighbouring blocks. This method enables the design to be efficiently divided into detailed design tasks with their own independent requirements; beneficial on large design projects requiring large interdisciplinary design

teams. The top down design approach is a standard technique, not something created by ISO26262; what the standard does add to it is the consideration of safety requirements and goals elicited from a hazard analysis and risk assessment.

The specific safety requirements and goals can be assessed in the same way as the functional requirements and goals to create a functional safety concept. This document explains how the design will ensure that all safety goals are met, creating actions on the product design and validation to ensure risk is at an acceptable minimum.

The middle section of the cycle covers the product development. This contains the detailed system and subsystem design and validation including integration testing as well as planning for the production and ongoing operations functions. As with the concept phase, the standard assumes a structured design methodology. This takes the form of the 'V-Cycle' as shown in Figure 5. The detail of the V-Cycle and the specific sub-system cycles was discussed further in chapters 3 and 4. In summary, the standard adds in work products to the V-Cycle to drive adequate safety analysis and validation of the design. Aiming to ensure that all safety goals are met and thus risk to the end user of the product is kept to an acceptable level.

The bottom section of the cycle deals with the production and operation of the product covered in detail in part 7. This is nearing the end of the design cycle and contains work products to monitor that the design is accurately realised. This section also looks briefly at post design change management – indicating the point at which a change should force the design to re-enter the life cycle.

Part 2 also prescribes how the project and organisational management should contribute to functional safety, discussing a 'safety culture' which must be incorporated into a business and design team. This covers the introduction of 'safety managers' for product, system, sub-system, customer and supplier designs and interfaces. It also describes the need for adequate employee training as well as the monitoring and auditing of projects to maintain compliance to the standard.

2. Part 3: Concept Phase

As previously described, the concept phase covers the progression of the project from its initial requirement elicitation up to the point of a block level concept design. In terms of the deliverables required by ISO26262 this section has 3 sections, the first being the initiation of the lifecycle. At the outset of a lifecycle there is scope to tailor it for a specific product or application. The inclusion or exclusion of any particular part of product of the cycle is justified by the completion of an impact analysis. This clearly defines the products of the lifecycle which are affected by a change or are relevant to the new design and so which must be produced. The second deliverable required to initiate the lifecycle is a safety plan; a definition of which products are to be produced when and by whom.

The second block within the concept design section of the lifecycle is the hazard analysis and risk assessment. This can be seen as the key to the entire functional safety concept; this analysis sets out to define all hazardous situations which can occur during the product operation or malfunction and to assign each one an Automotive Safety Integrity Level (ASIL). The standard suggests tools such as brainstorming, FMEA, quality

history and field studies to help extract the relevant hazards to be classified. There are then four ASILs rated from A to D into which each must be categorised; where A is seen as the least hazardous and so given least stringent controls and D is seen as most severe and has a higher level of control placed upon it. The ASIL for a particular hazard is chosen based on 3 separate subjective factors.

1. Severity; the severity of the potential injury attributed to the hazard is given a rating from S0 to S3 as shown in Figure 41.

	Class			
	S0	S1	S2	S3
Description	No injuries	Light and moderate injuries	Severe and life-threatening injuries (survival probable)	Life-threatening injuries (survival uncertain), fatal injuries

Figure 41: Severity ratings [4]

2. Probability; the likelihood of an event occurring is given a rating from E0 to E4 as shown in Figure 42.

	Class				
	E0	E1	E2	E3	E4
Description	Incredible	Very low probability	Low probability	Medium probability	High probability

Figure 42: Probability ratings [4]

3. Controllability; the final rating refers to the likely ability of the user to control the hazard to a safe conclusion. This is rated from C0 to C3 as shown in Figure 43.

	Class			
	C0	C1	C2	C3
Description	Controllable in general	Simply controllable	Normally controllable	Difficult to control or uncontrollable

Figure 43: Controllability ratings [4]

The 3 subjective ratings are then used to determine an ASIL as shown in Figure 44. Also appearing in this figure is the rating QM; this denotes that the ratings are sufficiently low enough that no action is required above that normally expected by an adequate quality management system. A safety goal must then be established for each ASIL rated hazard which can then be met by the design and verified.

Severity class	Probability class	Controllability class		
		C1	C2	C3
S1	E1	QM	QM	QM
	E2	QM	QM	QM
	E3	QM	QM	A
	E4	QM	A	B
S2	E1	QM	QM	QM
	E2	QM	QM	A
	E3	QM	A	B
	E4	A	B	C
S3	E1	QM	QM	A
	E2	QM	A	B
	E3	A	B	C
	E4	B	C	D

Figure 44: ASIL determination [4]

The final part of the concept phase then takes these hazards and safety goals and creates a functional safety concept around them. For example, if hazard 1 was given ASIL D status then the safety goal may be to transition

to a safe state within X seconds. The safety concept would capture this and then define is slightly more detail the mechanisms required to do so i.e. detect the presence of any fault which causes hazard 1 with Y seconds and implement a mechanism to remove the fault or hazardous condition within Z seconds where Y+Z<X. The functional safety concept can then be related to the design block diagram and all relevant goals and requirements can be applied to each module. The result of this may be the inclusion of monitoring circuitry or software detection algorithms during the design phases should analysis highlight a component fault be found which could lead to a particular hazard.

3. Part 4: Product Development at the System Level

The system level design is the first project stage where a technical concept is offered to the meet the functional and safety requirements. This part of ISO26262 makes the assumption that a V-Cycle will be used for this phase, this cycle feeds into the sub-system V-cycles described in the next section. The standard shows this in its simplest form with only two subsystems; hardware and software. However in reality there could be a complex system with multiple subsystems each with their own V-cycle within this one, the concept still remains the same.

The standard V-cycle concept can be seen in Figure 45. The left hand side of the V progresses through each expected design phase from planning and initiation, through requirements capture and analysis to the technical design. The right hand side then deals with the build and integration of the product and its testing, validation and assessment before managing the final release into production.

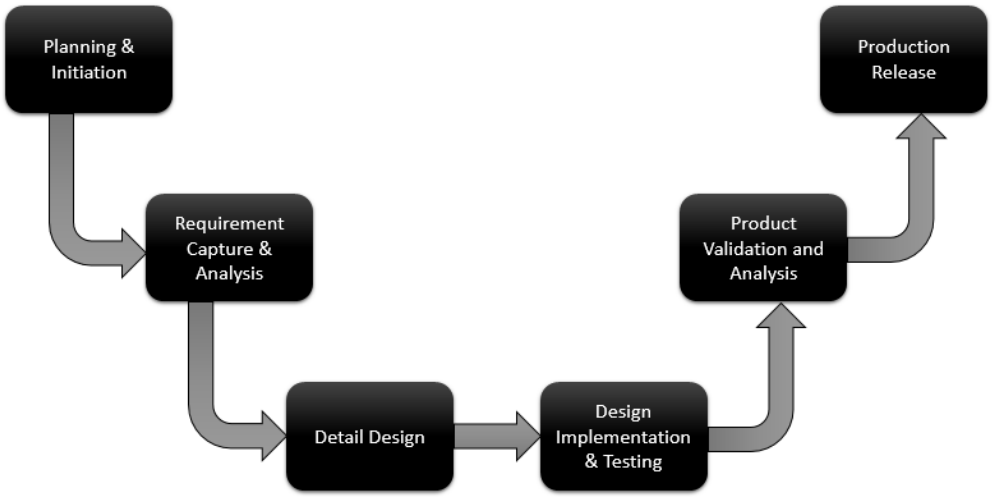

Figure 45: : Product design v-cycle

The ISO 26262 content diagram (Figure 5) shows how the authors have adapted the standard design cycle to show the safety deliverables and requirements at each phase. These deliverables are described in more detail in part 4 of the standard.

The first being the initiation of the system design phase, the specific work products for the first section are all planning related. These comprise of a refined project plan, a refined safety plan, an integration and test plan, a validation plan and a functional safety assessment plan.

Next comes the specification of technical safety requirements; a further refinement of the requirements placed on the system following the definition of safety goals in the functional safety concept. This is a complex process which considers the initial product architectural assumptions and looks to define safety mechanisms, applying the relevant requirements on modules

and interfaces. This section of the safety cycle also attempts to address the potential for latent faults; undetected faults which do not result in a hazardous situation when taken in isolation or under some operating conditions, but may prove hazardous in specific conditions or worsen the effect of other faults ordinarily deemed not to be severe or hazardous. A document defining these requirements is the primary work product of this section of the cycle, however a refinement to the validation plan and an assessment by analysis into the coverage of the safety goals by the safety requirements are also products of this phase.

The system design phase follows from the specification of functional requirements. In terms of the product design this is the definition of each subsystem and how they must interact in order for the system to meet all of requirements placed upon it. The ISO26262 [5] requirement on this phase mirrors this but from a safety perspective. In simple terms this means the definition of how each subsystem must respond in certain fault conditions and how these conditions must be tested and communicated between modules. As with previous phases, a deliverable of the system design phase is also an analytical verification that the design itself will satisfy each of the safety requirements. This analysis can be backed up using a combination of design tools, a commonly used tool is failure mode effect analysis (FMEA). This is an assessment which records all possible failures of each component within a system or sub-system along with their effect or reaction. It can then be used to target verification testing and the test results are often used as an argument to adjust the occurrence or

severity rating of each fault. An FMEA can then be used as an input and evidence for overall reliability calculations.

4. Part 5 & 6: Product Development at the Hardware and Software Levels

The detail design of the system level described in the previous section involves the specification of requirements for each sub-system, either in hardware or software. According to ISO26262 [5], this set of requirements also includes the provision of safety goals and requirements for each subsystem. The subsystem product development stage is very much a repeat of the system level V-Cycle taking its input from the detail design stage and feeds back into the system level design implementation and testing. Figure 46 shows the definition of the hardware level as described in the standard for reference. It can be seen that the sections of the sub-system design flow can be equated to the equivalent system level blocks and the standard 'V' design cycle.

The first section is 'Initiation of product development at the hardware level'; this section directly mirrors the first section of the system level design. This is the planning and initiation stage where the resource and schedule are put in place for the sub-system development.

Following this is the specification of hardware safety requirements, where the specific sub-system safety plan is defined based on the safety goals specified at system level. The importance of this section can be seen throughout the remainder of the sub-system development as all design and verification must be traced back to the requirements and goals defined and

documented in the work products in this stage. Another key requirement of this stage is the documented verification of these requirements against the system level goals and equivalent requirements, this proves that the design concept will satisfy the system level needs.

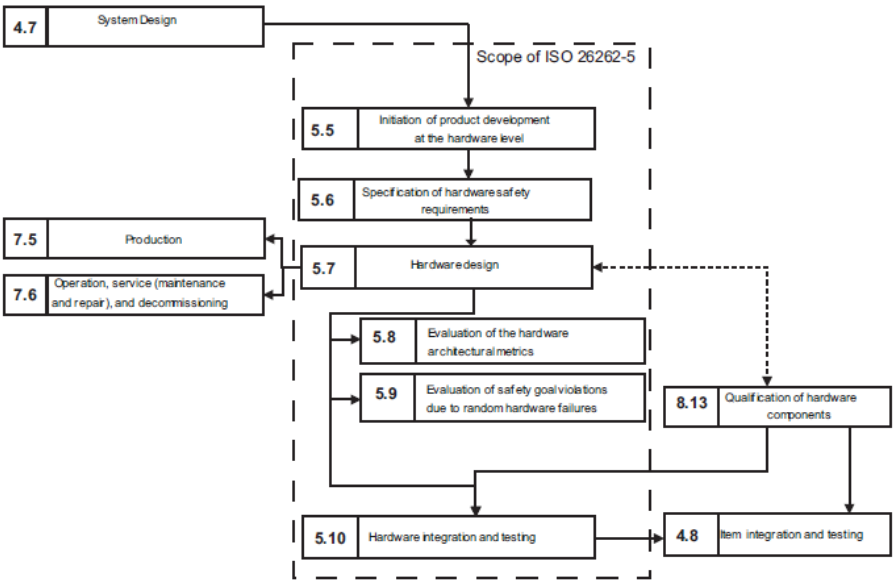

NOTE Within the figure, the specific clauses of each part of ISO 26262 are indicated in the following manner: "m-n", where "m" represents the number of the part and "n" indicates the number of the clause, e.g. "4.7" represents Clause 7 of ISO 26262-4.

Figure 46: Reference phase model for the product development at the hardware level

The hardware design section is then where the design is realised and if the sub-system is large and complex enough then further sub-system 'V' cycles could be defined. Design documentation is then required to link each safety goal and requirement to the design element in place to satisfy it. It is important in this section to maintain definition between the functional design and the safety design; the two overlap considerably however remain subtly different.

An example could be that of a simple 3 phase bridge to drive a motor, the functional design must enable adequate control of the motor by switching of the devices using sensible gate circuits designed for the entire range of operating conditions. This would require a worst case circuit analysis (WCCA) in order to guarantee its operation in varying environmental conditions and manufacturing tolerances. However, if there was a safety goal which stated that 'motor phase isolation must be possible under all conditions' this could not be guaranteed by the design analysis alone. In this scenario the safety goal would then drive a further design requirement which would likely force the addition of circuitry to ensure that motor isolation was always possible in any operating condition or under any reasonable fault condition. That safety goal would also likely drive the design of fault detection and reaction strategies, the documentation of which could also be offered to show compliance to this section of the standard.

The remaining sections within this part of the standard refer to the sub-system verification. As can be seen in Figure 46, these are all effectively parallel tasks and do in fact sometimes combine into one set of verifications, the aim here is to verify that the safety design effectively meets the safety goals and requirements. A possible way to do this is to take an output from the FMEA, highlighting all possible conditions which could cause a violation of the safety goal if not mitigated and create that condition in a controlled test to prove that the sub-system or system response is actually safe. This method of testing is referred to as fault insertion testing (FIT) and is often used as evidence for the safe operation of systems under extreme and fault conditions. The FIT results can then be referenced within the FMEA as a

verification of the predicted reaction and so completing the safety design V-cycle.

This is the final demand set out by the standard on the design phase, the following sections place demands on production and operations to ensure safe manufacture and service of any product developed for automotive applications. This thesis is oriented around the concept and design phases of the engineering V-cycle and so the final sections will not be covered.